## Reply to reviewer #1 of "Sensitivity of warm clouds to large particles in measured marine aerosol size distributions – a theoretical study"

Tom Dror[1], J. Michel Flores[1], Orit Altaratz[1], Guy Dagan[2], Zev Levin[3], Assaf Vardi[4], and Ilan Koren[1]

[1]Department of Earth and Planetary Sciences, Weizmann Institute of Science, Rehovot, Israel.

[2]Atmospheric, Oceanic and Planetary Physics, Department of Physics, University of Oxford, Oxford, UK.

[3]School of Earth Sciences, Department of Geophysics, Tel Aviv University, Ramat Aviv, Israel.

[4]Department of Plant and Environmental Sciences, Weizmann Institute of Science, Rehovot, Israel.

**We are grateful for the time and effort the reviewer invested in our work, and highly appreciate all of the constructive comments that helped us improve the paper. Below we address all the reviewer's comments point by point (our answers are marked in blue).**

In this paper, an axisymmetric cloud model with detailed bin–microphysics was initialized with six marine aerosol size distributions (MSD), measured in-situ in the Atlantic Ocean, Caribbean Sea and Pacific Ocean to study the effect of aerosol concentration and size distribution on warm clouds' properties. It shows that the cloud mass and precipitation change non-monotonically with the total concentration and size distribution of cloud condensation nuclei (CCN), especially when a tail of giant or ultragiant CCN (GCCN or UGCCN) is also included in the aerosol size distribution. The most interesting finding is the upper boundaries of the GCCN. This has not been reported in previous studies, to the best of my knowledge. The study is well within the scope of ACP and is generally well presented, except for a few places need to be clarified or corrected.

We thank the reviewer for the careful reading of our manuscript and this positive description of our work. We hope that the physical boundaries on GCCN will be helpful for the community.

**Specific comments:**

**1)** In the abstract, the statements and explanations are mainly based on the simulation results using the deepest thermodynamic profile, a more generalized statement or results including the shallower clouds should also be included, for a more complete picture.

**Authors reply:** We thank the reviewer for this important comment that helped us present our study in a more general way. We changed the abstract (and other parts in the paper, as described in answer no. 5) to describe the results of the different profiles.

The revised **abstract** reads: "Aerosol size distribution has major effects on warm cloud processes. Here, we use newly acquired marine aerosol size distributions (MSD), measured *in-situ* over the open ocean during the *Tara* Pacific expedition (2016—2018), to examine how the total aerosol concentration ($N_{tot}$) and the shape of the MSD change warm clouds' properties. For this, we used a toy-model with detailed bin-microphysics **initialized using three different atmospheric profiles, supporting the formation of shallow to intermediate and deeper warm clouds.** The changes in the MSDs affected the clouds' total mass and surface precipitation. In general, the clouds showed higher sensitivity to changes in $N_{tot}$ than to changes in the MSD's shape, except for the case where the MSD contained giant and ultragiant cloud condensation nuclei (GCCN, UGCCN). For increased $N_{tot}$ **(for the deep and intermediate profiles),** most of the MSDs drove an expected non-monotonic trend of mass and precipitation **(the shallow clouds showed only the decreasing part of the curves with mass and precipitation monotonically decreasing).** The addition of GCCN and UGCCN drastically changed **the non-monotonic trend**, such that surface rain saturated and the mass monotonically increased with $N_{tot}$. GCCN and UGCCN changed the interplay between the microphysical processes by triggering an early initiation of collision-coalescence. The early fall-out of drizzle in those cases enhanced the evaporation below the cloud base. Testing the sensitivity of rain yield to GCCN and UGCCN revealed an enhancement of surface rain upon the addition of larger particles to the MSD, up to a certain particle size, when the addition of larger particles resulted in rain suppression. This finding suggests a physical lower bound can be defined for the size ranges of GCCN and UGCCN."

**2)** I suggest each of filled circles in Fig. 2 (c)(d) to be marked with a time. The current figures are a little bit confusing.

**Author reply:** We thank the reviewer for this comment that helped us make the figure clearer. In the revised Fig. 2 (see below), we marked the filled circles on the black and blue curves, to indicate the simulated time (in *min*).

We also added specific time references to the part of the revised *Results* where Fig. 2 is interpreted to make it easier to follow the trajectories in the figure, **(section 3, L157—L161):** "At a later stage in the cloud's lifetime, the trajectories turn diagonally up **(~56 *min* into the simulation)**, showing that the collection process has begun. Finally, the clouds stop growing by condensation, reaching their maximum mass, and begin to evaporate **(~71 *min* into the simulation;** trajectories turn to the left). In the *Atlantic—1* MSD case, the collection process kicks in earlier, within 10 minutes of the cloud's lifetime **(~51 *min* into the simulation)**, due to the presence of GCCN in the MSD which initially form bigger droplets."

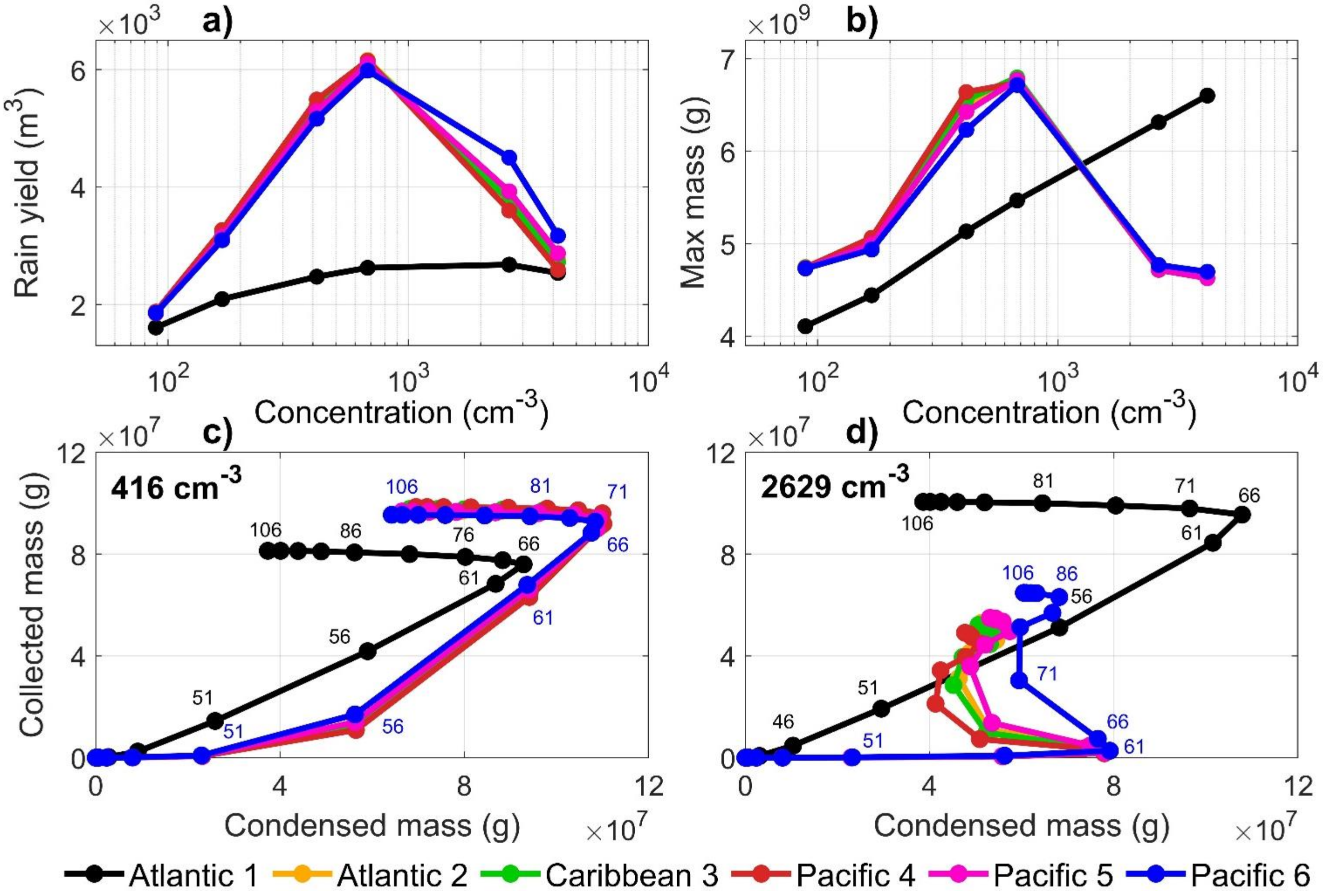


*Figure 2.* ***(a)*** *Surface rain yield and* ***(b)*** *cloud's maximum mass as a function of* $\mathbf{N_{tot}}$ *used in the simulation****, integrated over 150 minutes of simulations****. Each curve represents six simulations, done with a specific shape of the MSD normalized to different aerosol concentrations. The lower panels* ***(c, d)*** *show the time evolution of accumulated collected mass versus accumulated condensed mass.* ***The simulated time is noted along the black and blue curves for the Atlantic—1 and Pacific—6 MSDs, respectively.*** *The panels represent an aerosol concentration of 416 and 2629 cm$^{-3}$ (**c** and **d**, respectively).*

**3)** Line 183-184: "The *Atlantic-1* raindrops are considerably smaller than those produced by the other clouds (Fig. S6), and their evaporation is therefore greater": One fact might also be important is that while raindrops formed earlier in case *Atlantic-1*, the cloud is still in its developing stage, or the vertical velocity is still positive below cloud base, and the relative humidity is relatively low, so the raindrops spend more time and therefore evaporate more before reaching the surface. In other cases, rain was promoted by stronger downdrafts, and the relative humidity should also be higher. Therefore, it may provide more evidence to explain the differences in surface rain amount and evaporation mass between case *Atlantic-1* and other cases by analyze the below-cloud vertical velocity and relative humidity.

**Author reply:** We thank the reviewer for this important comment that allowed us to be more thorough in our explanation. We added to the SI a new figure (Fig. S7, attached below) that shows the time-height evolution of the horizontal mean values of cloud mass mixing ratio (Fig. S7a—b), droplet number concentration ($N_d$, Fig. S7c—d), vertical velocity ($w$, Fig. S7e—f), and relative humidity ($RH$, Fig. S7g—h) for all the cloudy (and rainy) pixels of the *Atlantic—1* and *Pacific—6* MSDs for an aerosol concentration of 2629 $cm^{-3}$. Note that the *RH* panels show only the sub—cloud layer to address the reviewer's comment. Focusing on the *w* and *RH* panels, they show clearly that the reduced surface rain of the *Atlantic—1* case is indeed due to a combination of the smaller raindrops, and their early fallout while the cloud is still in its developing stage. Therefore, the sub—cloud layer is dominated by updrafts and low *RH* values in comparison to the *Pacific—6* MSD (presented in this figure as a representative of all other MSDs).

We added an explanation to the *Results* **(section 3, L200—L205)**: "The *Atlantic—1* raindrops are considerably smaller than those produced by the other clouds (Fig. S6; see below), and their evaporation is, therefore, **more efficient**. **Moreover, the rain falls below the cloud base earlier, compared to the other MSDs cases, while the cloud is still in its developing stage, meaning that the cloud and the sub—cloud layers are dominated by updrafts, and the sub—cloud layer is consequently drier (Fig. S7). The combination of the small raindrops with their early fall out that lasts longer (due to the updrafts prevailing at this stage), results in greater rain evaporation below the cloud base for the *Atlantic—1* MSD."**

We also added the following explanations to the *Summary* **(section 4, L265—L268):** "This results in **the** fast formation of large drops and the early fall-out of drizzle **while the cloud is still in its developing stage, such that updrafts prevail and the sub—cloud layer is drier. The combination of a sub—cloud layer that is dominated by updrafts and features lower *RH* values, further promotes longer fall time for the small raindrops and an efficient evaporation below the *Atlantic—1* cloud base."**

**4)** Figure 4(e) and 4(f) show a little bit strange here and do not add more support to the main body of the text, may be removed?

**Author reply:** While we agree that these two images are exceptional in this paper, we believe they are a valuable addition. They emphasize the uniqueness of this work that relies on *in-situ* measurements as the initial conditions for the modeled aerosol's MSDs, while also showing the type and size of big aerosol (GCCN and UGCCN) that are present in the marine boundary layer. However, following the reviewer's comment and to better explain them we separated panels e—f from Fig. 4 and put them in a separate new Figure (Fig. 5, see below) in the *Summary* (section 4) of the revised manuscript, where we want to demonstrate which type of GCCN and UGCCN were measured over the open ocean.

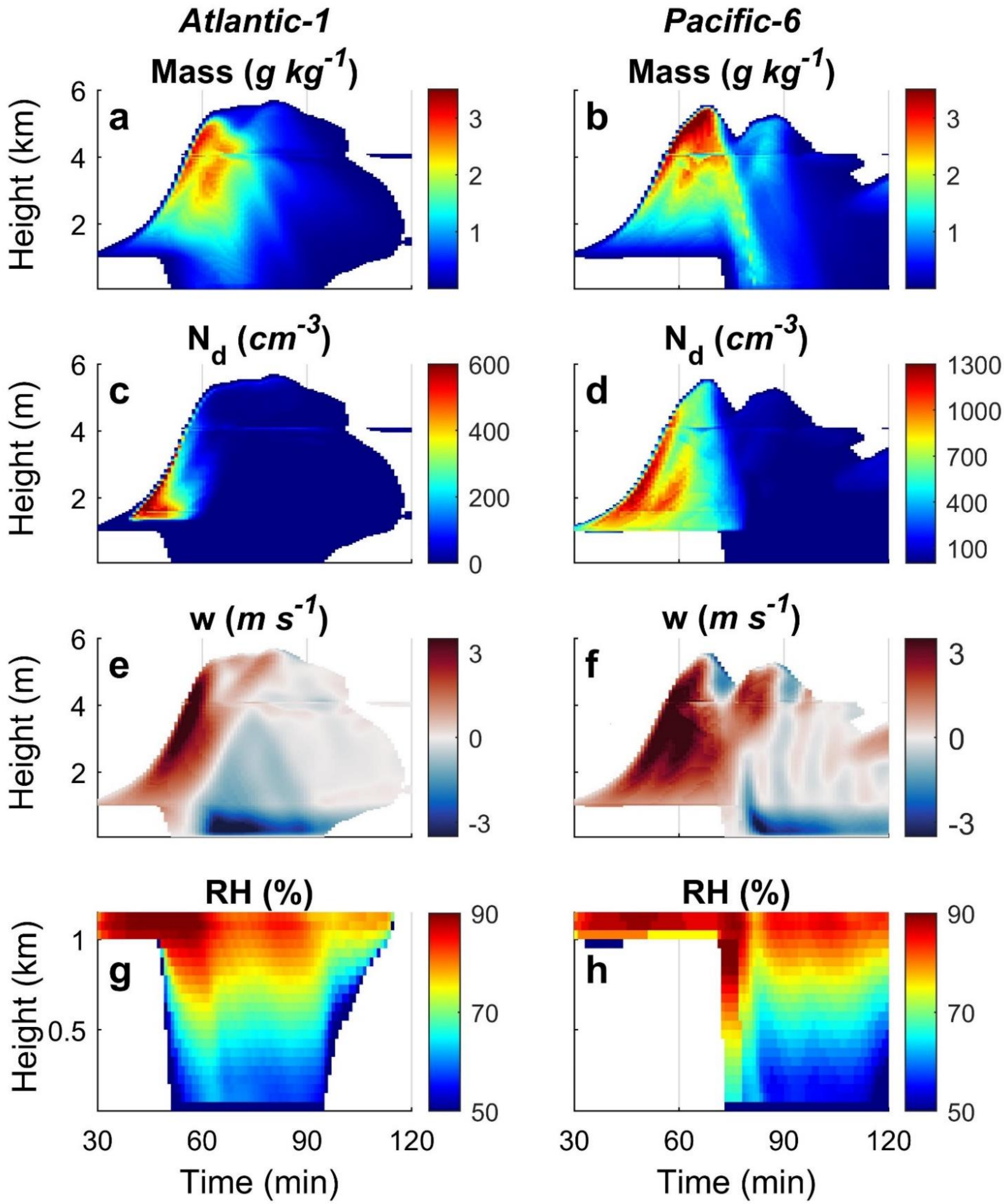


*Figure S7. Time-height diagram of the horizontal mean of* ***(a, b)*** *cloud mass mixing ratio (g kg$^{-1}$),* ***(c, d)*** *droplet number concentration ($N_d$, cm$^{-3}$),* ***(e, f)*** *vertical velocity (w, m s$^{-1}$), and* ***(g, h)*** *relative humidity (RH, %) below the cloud base, for the Altantic-1 (left column) and Pacific-6 (right column) MSDs normalized to an aerosol concentration of 2629 cm$^{-3}$. Values are shown only for the cloudy (and rainy) pixels (mixing ratio > $10^{-3}$ g kg$^{-1}$). Note the different scales for the color bars in panels* ***(c)*** *and* ***(d)****.*

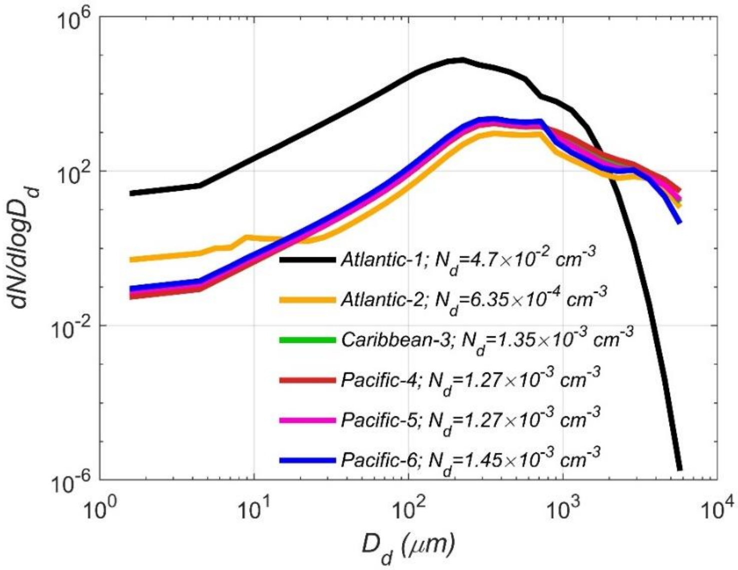


*Figure S6. Droplet size distribution below the cloud base at the time of maximum surface rain rate for the six different MSDs normalized to $N_{tot}$ = 2629 $cm^{-3}$. The total droplet number concentration ($N_d$, $cm^{-3}$) is noted in the legend for each MSD.*

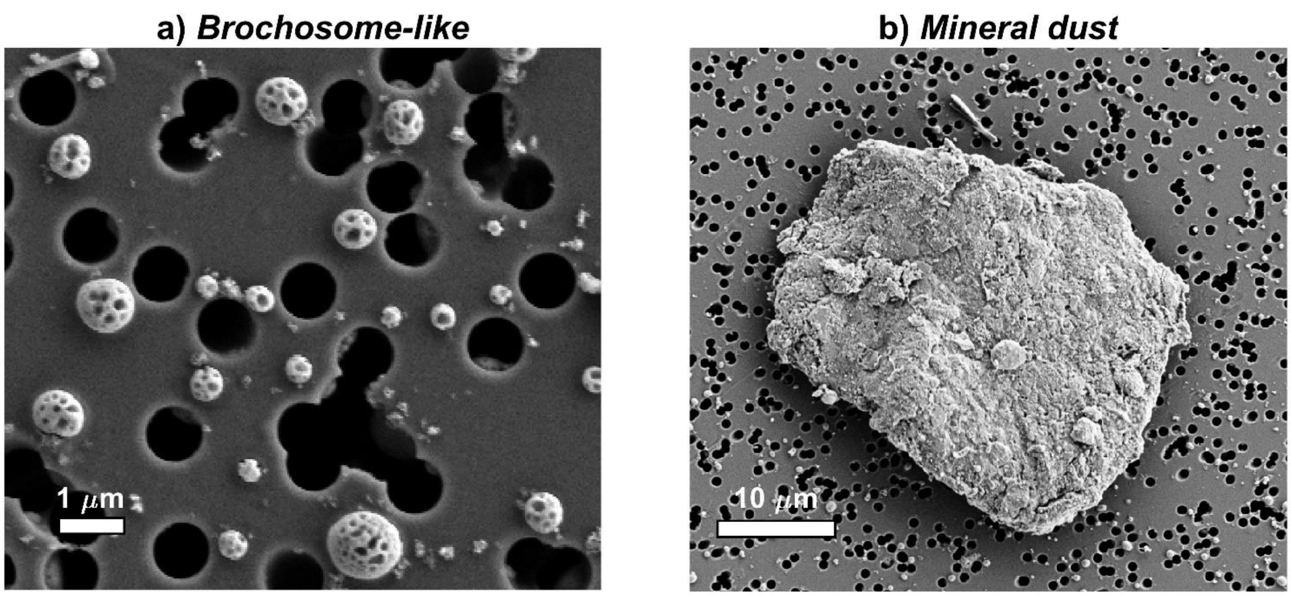


*Figure 5. Scanning electron microscope images of Brochosome-like particles (a), and mineral dust (b) collected during the same period as the Atlantic-1 MSD measurement.*

**5)** In this paper, only results from the simulation with the most unstable thermodynamic profile are analyzed in detail. For shallower clouds, the rain yield and the max. cloud mass show monotonic change with CCN concentration and no significant changes with GCCN. So the conclusion should be generalized to reflect how the results change for other thermodynamic situations.

**Author reply:** We thank the reviewer for this comment. Based on this and to give a more general picture of our results, we changed the abstract to describe the other profile's results as well (see answer no. 1

above). In addition, we added more explanations regarding the intermediate and shallow profiles to other parts of the manuscript.

*Results* **(Section 3, L121—126):** "The general shape of the five curves is similar **for the deep and intermediate profiles**, and exhibits a non-monotonic trend (see Fig. 2a—b **and Fig. S2a—b, respectively**): an increase in total rain yield and the cloud's maximum mass as a function of aerosol loading, up to a maximum optimal aerosol concentration ($N_{op}$), followed by a decrease. All five curves have a similar $N_{op}$ of around $N_{tot} = 677\ cm^{-3}$ **($N_{tot} = 416\ cm^{-3}$ for the intermediate profile)** for both surface rain yield and maximum cloud mass. **For the shallow profile, the five MSD curves preset only the decreasing branch, with a minor decrease in rain yield and cloud mass with increasing aerosol loading.**"

*Results* **(Section 3, L135—139):** "For the cases of shallower cloudy-layers, where the clouds are more subjected to entrainment effects, the ascending branch of the curves is less pronounced (**intermediate profile,** Fig. S2a—b) or non-existent (**shallow profile,** Fig. S2c—d). We, therefore, focus on the deepest atmospheric profile, which better demonstrates the full effect of the competition and interactions between the microphysical processes in the clouds, **and refer to Text S2 in the SI for the intermediate and shallow profiles."**

*Summary* **(Section 4, L250—254):** "We focused on the deepest profile, since it best captured the effect of competing microphysical cloud processes, and showed that surface rain yield and cloud's maximum mass are affected in a non-monotonic way by changes in $N_{tot}$, and the shape of the MSDs for most of the cases. **This was also the case for the intermediate profile results, while the shallow one only showed the decreasing branch of this non-monotonic trend, due to more dominant entrainment effects.**"

***Text S2. Additional Atmospheric Profiles*** in the SI was extended and now includes the following (L29—L36): "We examined the surface rain yield and the cloud's maximum mass as a function of $N_{tot}$. The results of the deepest cloud profile are shown in the main text (Fig. 2a—b), and the other two profiles are shown in Fig. S2. **The trends of the *Atlantic—1* surface rain yield and cloud's maximum mass curves for the intermediate profile are similar to the ones of the deeper profile. The only difference is that the rain yield values of the *Atlantic—1* are higher than the ones produced by the other MSDs for $N_{tot} > 677\ cm^{-3}$. All the curves show a lower $N_{op}$ compared to the deepest profile curves. Under the shallow thermodynamic profile, the *Atlantic—1* rain yield curve shows a similar trend to all other MSD cases, while producing the highest rain values. As for the trend in cloud mass, the *Atlantic—1* shows a monotonic increase (similar to the deep and intermediate profiles).**"

**Technical corrections:**

**1)** Line 143, change "accumulating" to "accumulated";

**Author reply:** Changed.

**2)** Line 206: Figure 4b,d should be "Figures 4b-d.

**Author reply:** Corrected.

# Reply to reviewer #3 of *"Sensitivity of warm clouds to large particles in measured marine aerosol size distributions – a theoretical study"*

Tom Dror[1], J. Michel Flores[1], Orit Altaratz[1], Guy Dagan[2], Zev Levin[3], Assaf Vardi[4], and Ilan Koren[1]

[1]Department of Earth and Planetary Sciences, Weizmann Institute of Science, Rehovot, Israel.

[2]Atmospheric, Oceanic and Planetary Physics, Department of Physics, University of Oxford, Oxford, UK.

[3]School of Earth Sciences, Department of Geophysics, Tel Aviv University, Ramat Aviv, Israel.

[4]Department of Plant and Environmental Sciences, Weizmann Institute of Science, Rehovot, Israel.

**We are grateful for the time and effort the reviewer invested in our work, and highly appreciate all of the constructive comments that helped us improve the paper. Below we address all the reviewer's comments point by point (our answers are marked in blue).**

The influence of aerosol size distribution and chemical composition on precipitation formation and intensity is still a challenging question to answer, due primarily to the sophisticated microphysical processes dealing with particles with a wide range of sizes, and also to the interplays between dynamics and microphysics. In this study, the authors choose to focus on addressing aerosol-precipitation response in a warm cloud, using a detailed bin microphysical framework for both aerosols and cloud droplets while a somewhat simplified dynamical framework (an axisymmetric model). In addition, they have also assumed a uniform chemical composition for the included aerosol population (sea salt) to limit the aerosol activation in a one-dimensional (size) parametric space. In order to address the targeted issue more realistically, they have also adopted measured aerosol size distributions collected from locations with different atmospheric backgrounds.

An interesting finding of this study is the significant difference in aerosol-precipitation responses between a case with the so-called *Atlantic-1* aerosol profile with ultra large CCNs and cases with other measured aerosol profiles without evident fraction of such giant CCNs. With a careful design of their modeling simulations, the authors have been able to define the criterion size of large aerosol particles that can create significant impacts on precipitation. Overall speaking, the paper has been relatively well organized, the research findings are well presented, and conclusions are drawn with solid science evidence.

We thank the reviewer for the careful reading of our manuscript and the constructive remarks.

**1)** A clear missing information in the manuscript is the cloud droplets concentrations, especially the vertical profiles of number concentration of cloud droplets and raindrops.

… In addition, Fig. 2(d) presents a rather interesting feature in high concentration simulations using all the distributions except *Atlantic-1* where collision-coalescence overwhelmed the condensation growth in a relatively early stage. However, without information of vertical distributions of cloud mass, the reader would have problem to understand (1) why the collision-coalescence increases with time but in a rather slow pace comparing to the case of *Atlantic-1*, and (2) the depths of layer where cloud mass grew in various cases. Note that large droplets (i.e., raindrops) can still be moved upward by updraft and both condensation and collision-coalescence can proceed in either updraft or downdraft (as far as the parcel remains saturated). Therefore, knowledge of the vertical growth tracks of precipitating particles is critical to understand how the two major growing processes evolved.

**Author reply:** We thank the reviewer for these important comments. Here we address the reviewer's comments regarding the vertical profiles of number concentration of cloud droplets and raindrops, as well as the vertical distributions of cloud mass.

Following the reviewer's suggestion and to better explain our results, we added Text S7 and Figure S7 to the SI (see below) showing the time-height horizontal mean profiles of: cloud mass mixing ratio, droplet number concentration ($N_d$), vertical velocity ($w$), and relative humidity ($RH$) below the cloud base, for the *Atlantic—1* and *Pacific—6* MSDs, normalized to an aerosol concentration ($N_{tot}$) of 2629 $cm^{-3}$. We also added Text S8 and Figure S8 to the SI (see below as well) showing the time-height evolution of the horizontal mean profiles of the number concentration ($N_r$) and mass mixing ratio ($M_r$) of precipitating particles ($D_p > 80\ \mu m$) for the *Atlantic-1* and *Pacific-6* MSDs, normalized to $N_{tot} = 2629\ cm^{-3}$.

We chose to show the *Pacific—6* MSD results as a representative example since it represents well all the other four MSDs cases. As can be seen in Fig. R1 below, that shows the time-height evolution of the horizontal mean profiles of cloud mass mixing ratio for all the MSDs for $N_{tot} = 2629\ cm^{-3}$, there are only minor differences among the four clouds.

We added an explanation regarding this issue to the *Results* (**section 3, L169—L181):** "Under more polluted conditions, the trajectory of the *Atlantic—1* MSD cloud (black curve in Fig. 2d) on this phase space is similar (in shape) to the one in the cleaner case (black curve in Fig. 2c), but this cloud accumulates more mass, due to the larger droplet surface area (Fig. S5b—c). **However, the *Atlantic—1*'s total droplet surface area is lower in comparison to the rest of the clouds (see Fig. S5c), and still, it condenses more mass, reaching ~$11 \times 10^7$ *g* compared to ~$8 \times 10^7$ *g* as the rest of the clouds. This can be explained by the nucleation of the GCCN and UGCCN that are present in the *Atlantic—1* MSD under polluted conditions, which on the one hand accumulate more mass (Fig. 2d) and drive a significantly higher number of raindrops at the growing stage of the cloud (Fig. S8), and on the other hand, results in a lower droplet number concentration ($N_d$) compared to the other clouds (Fig. S7). Therefore, the vertical distribution of mass of the *Atlantic—1* cloud is dominated by the precipitating particles, unlike the other clouds (Figs. S7 and S8). Note that while the total cloud mass of the *Atlantic—1* is larger than the one obtained by the other clouds, it is in the same order of magnitude. However, the mass of precipitating particles in the *Atlantic—1* cloud overwhelms the ones exhibited by the other MSDs. Contrastingly, the $N_d$ of the other clouds is much higher than the one of the *Atlantic—1* cloud, allowing for collision-coalescence to begin toward the end of the condensational growth stage, or after the evaporation process has begun (e.g., *Pacific—4*, the trajectories turn back to the left before acquiring a vertical component), and to increase in a slow pace. For the *Atlantic—1* cloud, the accumulation of liquid water by nucleation and condensation occurs in parallel to the collection process that starts much earlier in this case (Fig. 2d).**"

We added ***Text S7. Time—height Diagrams of Cloud Mean properties*** to the SI **(L67—L76):** "**To understand the vertical distribution of some of the cloud's key properties, we show the time evolution of the cloud mass mixing ratio, droplet number concentration ($N_d$), vertical velocity ($w$), and relative humidity (*RH*) below the cloud base for the *Atlantic—1* and the *Pacific—6* MSDs normalized to $N_{tot}$ = 2629 $cm^{-3}$. We show the *Pacific—6* MSD case as a representative example to the other four MSD cases, since their results are very similar. It is clear that while the *Atlantic—1*'s mass is the same order of magnitude as the one of the *Pacific—6*, the total $N_d$ is considerably smaller for the *Atlantic—1* cloud, and that the droplets are confined to the lower part of the cloud. These are big droplets that nucleated on the GCCN and the UGCCN in the *Atlantic—1* MSD. These droplets sediment out almost immediately after their formation, thus are not carried to higher levels in the cloud. The *Atlantic—1* starts to precipitate earlier than the other clouds (as discussed in the main text), while the cloud is still in its developing stage, updrafts prevail and the sub—cloud layer features low *RH* values**."

We added ***Text S8. Time—height Diagrams of Precipitating Particle's Growth*** to the SI **(L77—L84): "For clarifying the reasons behind the reduced surface rain amounts that are observed in the *Atlantic—1* MSD case, Fig. S8 shows the time-height evolution of the horizontal mean profiles of raindrops number concentration $N_r$ ($D_p$ > 80 μm), and mass mixing ratio $M_r$ ($D_p$ > 80 μm), for the *Atlantic—1* and the *Pacific—6* MSDs, normalized to $N_{tot}$ = 2629 $cm^{-3}$. The formation of raindrops is observed at a very early stage of the *Atlantic—1* cloud lifetime, compared to the timing of the rain formation in the *Pacific—6* case. In addition, it is clear that the high $N_r$ around the *Atlantic—1*'s cloud base contains very little mass, but the drops are big enough to fall out. However, since the drops are small, and the sub—cloud layer is still dominated by updrafts (Fig. S7e—f) the majority of them evaporate before reaching the surface (efficient evaporation and longer fall time)."**

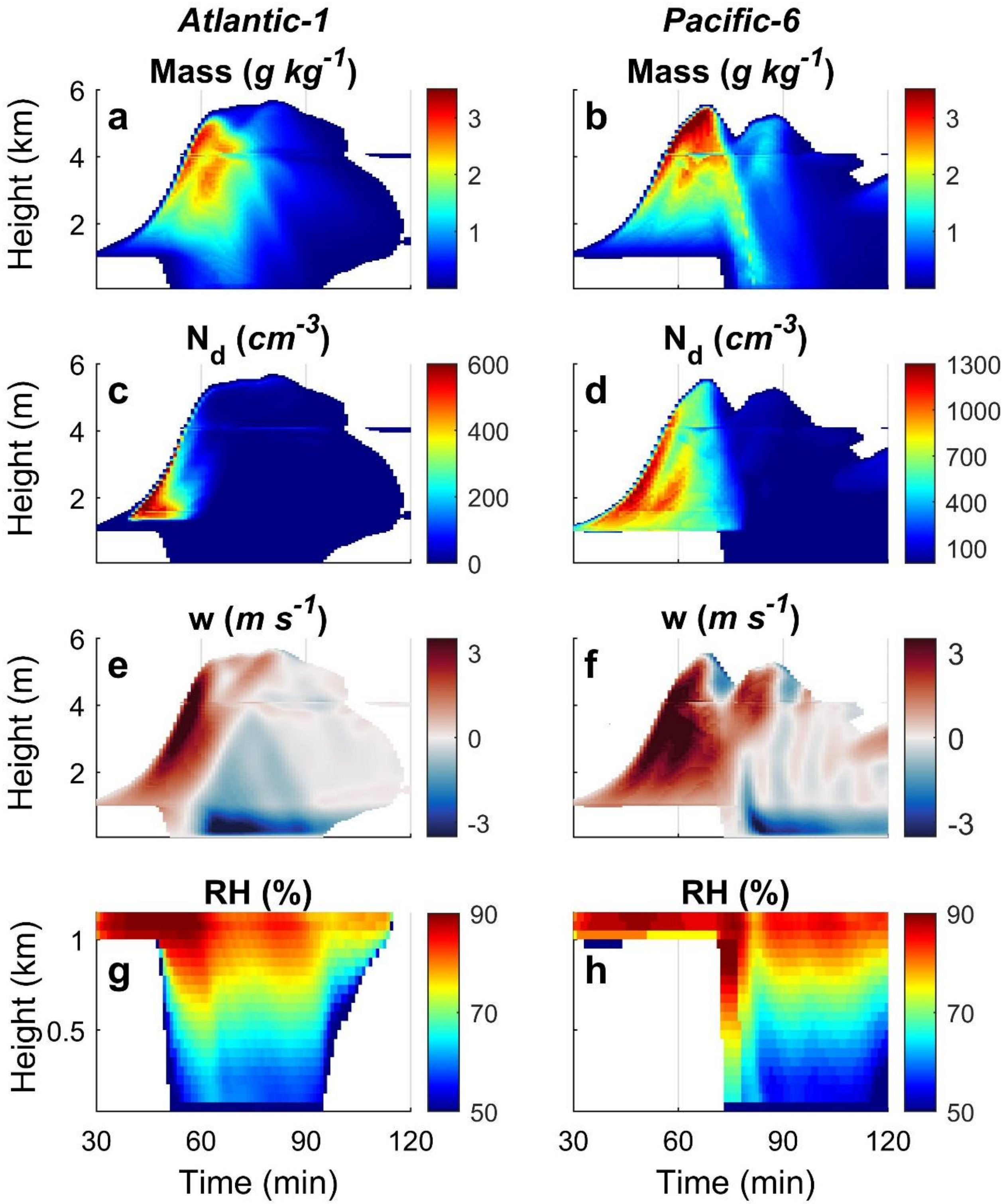


*Figure S7. Time-height diagram of the horizontal mean of **(a, b)** cloud mass mixing ratio (g kg$^{-1}$), **(c, d)** droplet number concentration ($N_d$, cm$^{-3}$), **(e, f)** vertical velocity (w, m s$^{-1}$), and **(g, h)** relative humidity (RH, %) below the cloud base, for the Atlantic—1 (left column) and Pacific—6 (right column) MSDs normalized to $N_{tot}$ = 2629 cm$^{-3}$. Values are shown only for the cloudy (and rainy) pixels (mixing ratio > 10$^{-3}$ g kg$^{-1}$). Note the different scales for the color bars in panels **(c)** and **(d)**.*

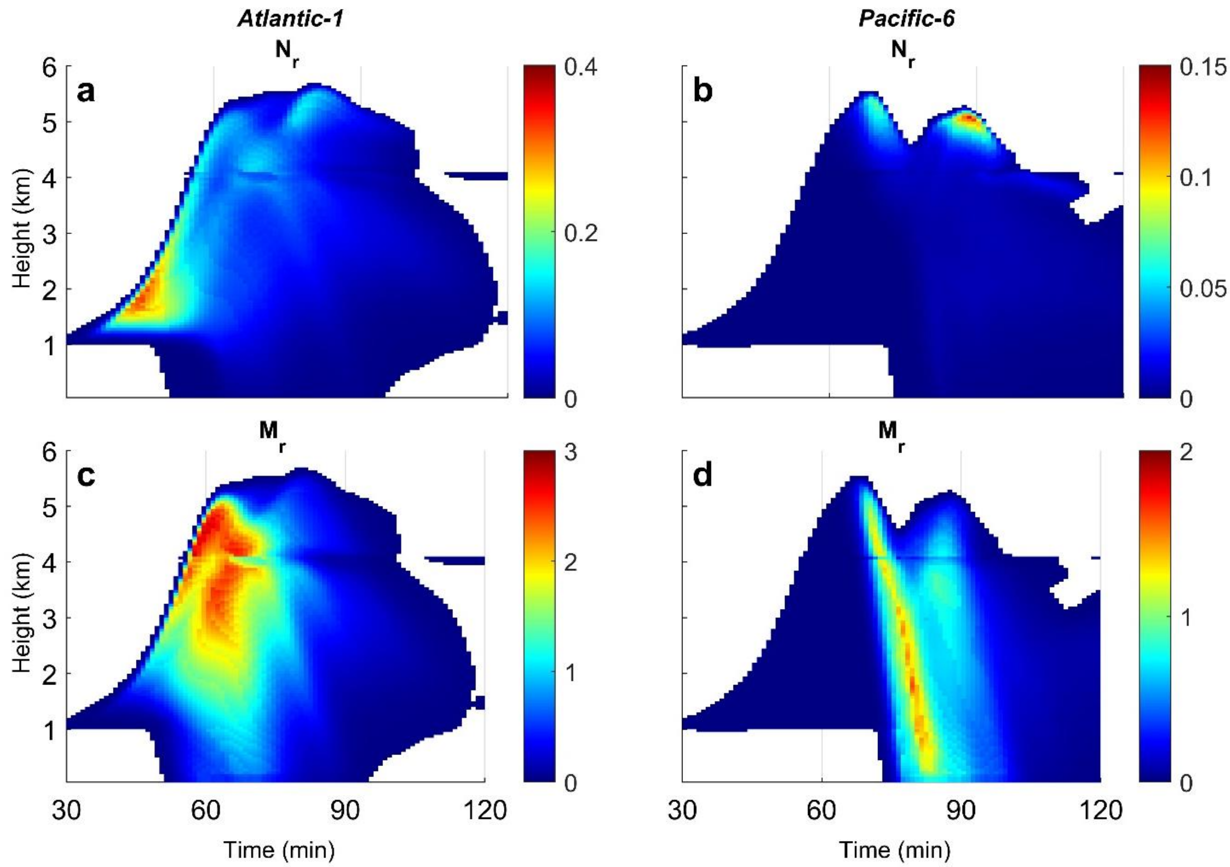


*Figure S8. Time—height diagram of the horizontal mean of raindrops ($D_p$ > 80 µm)* ***(a, b)*** *number concentration ($N_r$, $cm^{-3}$) and* ***(c, d)*** *mass mixing ratio ($M_r$, g $kg^{-1}$), for the Atlantic—1 (left column) and Pacific—6 (right column) MSDs normalized to $N_{tot}$ = 2629 $cm^{-3}$. Values are shown only for the cloudy (and rainy) pixels (mixing ratio > $10^{-3}$ g $kg^{-1}$). Note that the color bars have different limits for the Atlantic—1 and Pacific—6 clouds.*

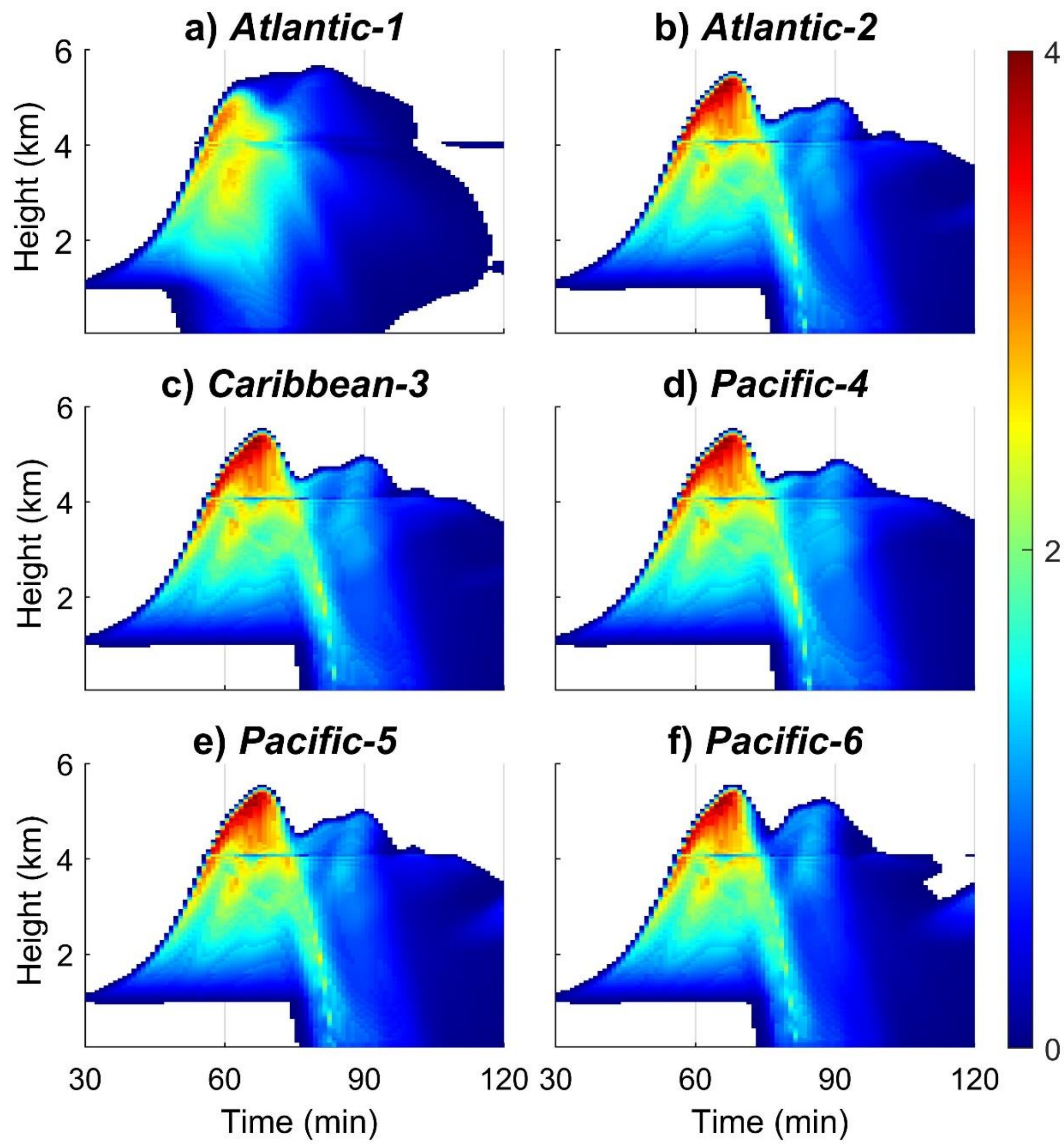


*Figure R1. Time-height diagram of the horizontal mean profiles of cloud mass mixing ratio (g kg$^{-1}$) for all MSDs for an aerosol concentration of 2629 cm$^{-3}$. There are only minor changes among all MSD's besides the Atlantic—1. We, therefore, took Pacific—6 as a representative MSD.*

**2)** The authors have discussed the correlation between sub-cloud evaporation and rainfall at surface. With a knowledge of sub-cloud raindrop population including total number and size distribution this would be much easier to understand.

**Author reply:** Thank you for this comment. The revised Fig. S6 (see below) shows the droplet size distribution below the cloud base at the time of maximum surface rain rate for the six different MSDs normalized to $N_{tot}$ = 2629 $cm^{-3}$. The total number concentration of droplets was added for the different curves. The figure clearly shows that the *Atlantic—1* MSD has more small raindrops and less big raindrops than the other MSDs.

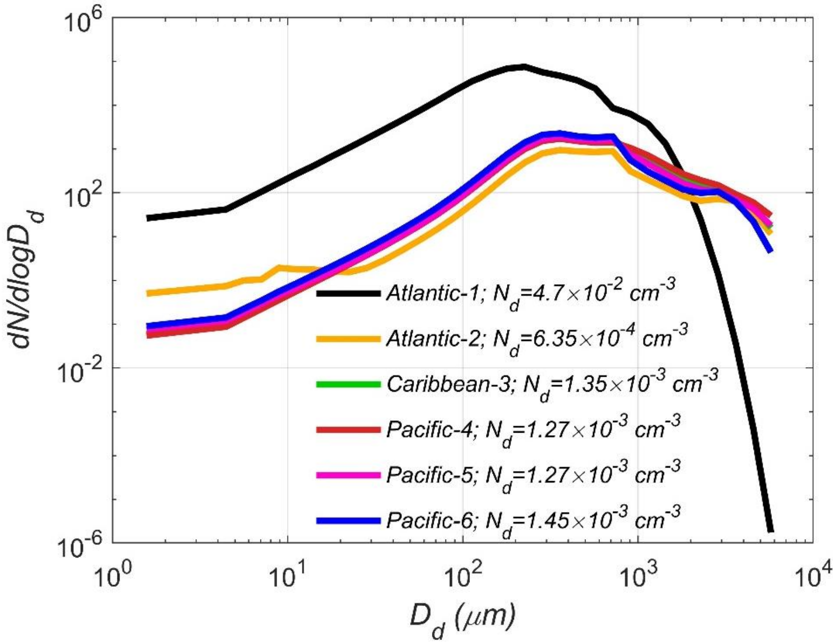


*Figure S6. Droplet size distribution below the cloud base at the time of maximum surface rain rate for the six different MSDs normalized to $N_{tot}$ = 2629 $cm^{-3}$. The total droplet number concentration ($N_d$, $cm^{-3}$) is noted in the legend for each MSD.*

**3)** It is understood that the authors wanted to focus on the aerosol and cloud microphysical connections. Nevertheless, the feedback of dynamics, even in a rather simplified dynamical framework still plays a role in determining the growth of precipitating particles. The authors mentioned very briefly about cold downdraft and also analyzed sub-cloud evaporation. Perhaps a more in-depth analysis would provide a better understanding of the role of dynamical feedback in, e.g., leading to the results presented in Fig. 3 and 4.

**Author reply:** We thank the reviewer for highlighting this important point. As described in answer no. 1 above, we are now showing the vertical velocity in the revised version of the SI in Fig. S7e—f. As the reviewer stated, the dynamics is strongly coupled to the microphysics, and hence it has a crucial effect on the growth of precipitating particles and now it is presented in the paper to create a full picture. The early fall-out of the smaller *Atlantic—1* rain drops, while the cloud is still in its developing stage, results in the *Atlantic—1* raindrops falling through updrafts that dominate the cloud and the sub-cloud layer at this stage (Fig. S7g—h). This causes a longer fall and together with the fact that the *Atlantic—1* sub—cloud layer is drier, promotes the efficient evaporation of the already smaller raindrops of the *Atlantic—1* cloud. This results in the reduced surface rain as shown in Figs. 3 and 4 of the main text.

To clarify this point in the main text, we added the following paragraph to the *Results* **(section 3, L200—L205)**: "The *Atlantic—1* raindrops are considerably smaller than those produced by the other clouds (Fig. S6; see below), and their evaporation is, therefore, **more efficient**. **Moreover, the rain falls below the cloud base earlier, compared to the other MSDs cases, while the cloud is still in its developing stage, meaning that the cloud and the sub—cloud layers are dominated by updrafts, and the sub—cloud**

**layer is consequently drier (see Fig. S7). The combination of the small raindrops with their early fall out that last longer (due to the updrafts prevailing at this stage), results in greater rain evaporation below the cloud base for the *Atlantic—1* MSD."**

We also added the following to the *Summary* **(section 4, L272—L275):** "This results in **the** fast formation of large drops and thus, an early fall-out of drizzle, **while the cloud is still in its developing stage, updrafts prevail and the sub—cloud layer is drier. The combination of a sub—cloud layer that is dominated by updrafts and features lower *RH* values, further promotes longer fall time for the small rain drops and an efficient evaporation below the *Atlantic—1* cloud base."**

**Some minor comments.**

**4)** Page 5, Figure 2(a) and (b): it would be helpful to provide the integration length of each simulation shown in these two figure panels in the figure caption.

**Author reply:** We added the integration length of the simulation (150 *min*) to the revised Fig. 2 caption.

**5)** Page 5, Ln 112: I understand the purpose of normalizing every distribution to match a given total concentration is for the convenience to identify the role of certain characteristics of size distributions such as shape in influencing the formation of precipitation. However, it is expected that the shift of the distributions to meet often much higher concentrations would increase the number of GCCN or even UGCCN. Could the authors provide such numbers even in the supplementary materials as a table or so? In addition, I don't remember this has been discussed in the manuscript, e.g., why the increase of GCCN still had no effect on the overall rain formation and growth for all cases including Atlantic-2 other than Atlantic-1.

**Author reply:** We thank the reviewer for this comment. As we normalize the MSDs to higher aerosol concentrations, we indeed shift the distributions such that they contain bigger particles (see Fig. S1 below). However, most of the MSDs (all except from the *Atlantic—1* and *Atlantic—2*) did not contain any GCCN or UGCCN even in the case of the highest $N_{tot}$. In the paper we define a physical threshold for GCCN ($D_p$~$5\ \mu m$) and UGCCN ($D_p$~$14\ \mu m$). These thresholds are marked on the revised panels of Fig. S1, for each $N_{tot}$. The *Atlantic—1* and the *Atlantic—2* are the only MSDs that contain GCCN, and the *Atlantic—1* is the only MSD that contains UGCCN. Even though the *Atlantic—2* contains some GCCN, they are present at low concentrations ($1.6x10^{-6}$—$7.5x10^{-5}\ cm^{-3}$, for the lowest and highest $N_{tot}$, respectively). These concentrations of GCCN are low in comparison to e.g., the GCCN concentration of the *Atlantic—1* ($1.9x10^{-5}$—$5.7x10^{-4}\ cm^{-3}$), and are not sufficient to cause any effect on the *Atlantic—2* rain formation and growth.

We added a clarification regarding this matter to *Methods* **(section 2.2., L109—111):** "**As we normalized the MSDs to higher values of $N_{tot}$, the MSDs shifted such that they contained larger particles (Fig. S1). However, only the *Atlantic—1* and *Atlantic—2* MSDs contained GCCN, and the *Atlantic—1* was the only MSD that contained UGCCN even in the case of the highest aerosol concentration.**"

We also extended ***Text S1. Normalized MSDs*** to include the following paragraph **(L17—L21):** "**The *Atlantic—1* and the *Atlantic—2* are the only MSDs that contained GCCN, and the *Atlantic—1* is the only MSD that contained UGCCN. Note that even though the *Atlantic*—2 contained some GCCN, they were present at low concentrations (*$1.6x10^{-6}$—$7.5x10^{-5}$ $cm^{-3}$*, for the lowest and highest $N_{tot}$, respectively). These concentrations of GCCN are low in comparison to e.g., the GCCN concentration of the *Atlantic—1* (*$1.9x10^{-5}$—$5.7x10^{-4}$ $cm^{-3}$*), and are not sufficient to cause any effect on the *Atlantic—2* rain formation and growth.**"

**6)** Page 7, Ln 152: "bigger droplets resulted in a lower total droplets' surface area. . .", the sentence is somewhat ambiguous since such a result is not obvious, an explanation would be helpful here.

**Author reply:** We thank the reviewer for this comment.

We clarified this in the revised *Results* **(section 3, L161—L164):** "The bigger droplets **formed by the nucleation of GCCN** resulted in a lower droplets' surface area **for a given total water mass (compared to the one that would have formed from droplets nucleated on smaller CCNs)** for the *Atlantic-1* MSD case and also compared to the other MSDs (Fig. S5). **The lower total droplets' surface area** was then further reduced by the early initiation of the collection process."

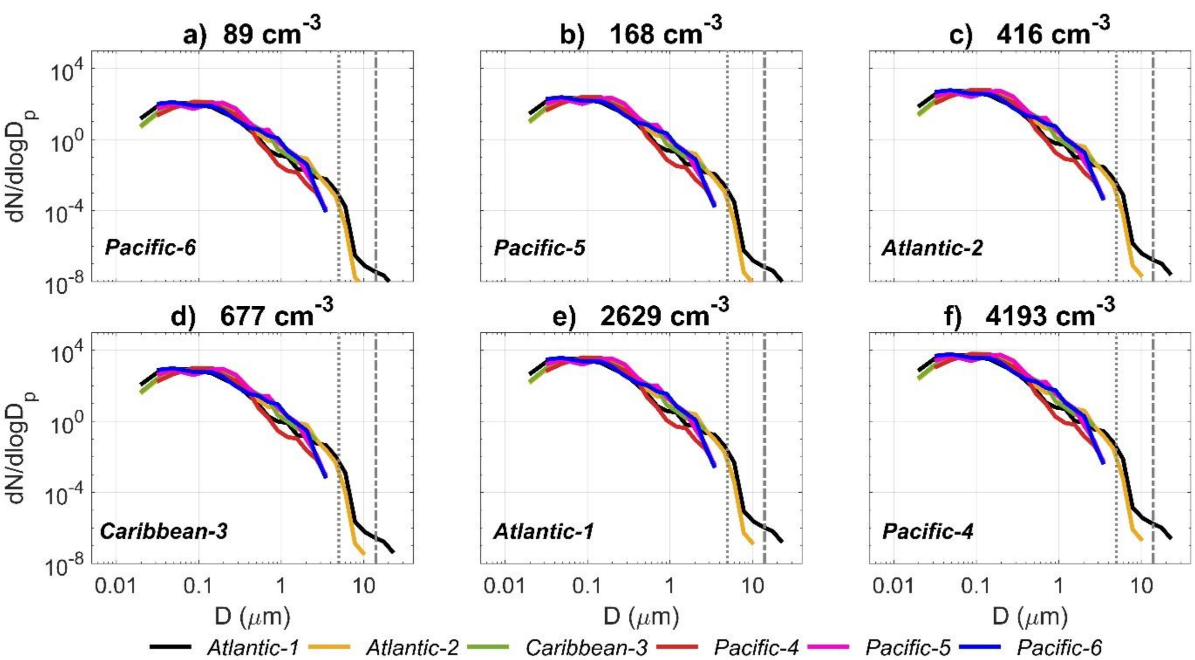


*Figure S1: All of the MSDs used in the model. Each panel shows the MSDs normalized to the specific total aerosol concentration of the MSD noted in the lower left corner. The panels are organized from clean **(a)** to polluted **(f)** conditions. **Dotted and dash-dotted verticals line indicated the threshold for GCCN ($D_p$~5 μm) and UGCCN ($D_p$~14 μm), respectively.***

# Sensitivity of warm clouds to large particles in measured marine aerosol size distributions – a theoretical study

Tom Dror[1,*], J. Michel Flores[1,*], Orit Altaratz[1], Guy Dagan[2], Zev Levin[3], Assaf Vardi[4], and Ilan Koren[1]

[1]Department of Earth and Planetary Sciences, Weizmann Institute of Science, Rehovot, Israel.
[2]Atmospheric, Oceanic and Planetary Physics, Department of Physics, University of Oxford, Oxford, UK.
[3]School of Earth Sciences, Department of Geophysics, Tel Aviv University, Ramat Aviv, Israel.
[4]Department of Plant and Environmental Sciences, Weizmann Institute of Science, Rehovot, Israel.
[*]Contributed equally to this work.

**Correspondence:** Ilan Koren (Ilan.koren@weizmann.ac.il)

**Abstract.** Aerosol size distribution has major effects on warm cloud processes. Here, we use newly acquired marine aerosol size distributions (MSD), measured *in-situ* over the open ocean during the *Tara* Pacific expedition (2016–2018), to examine how the total aerosol concentration ($N_{tot}$) and the shape of the MSD change warm clouds' properties. For this, we used a toy-model with detailed bin-microphysics initialized using three different atmospheric profiles, supporting the formation of shallow to intermediate and deeper warm clouds. The changes in the MSDs affected the clouds' total mass and surface precipitation. In general, the clouds showed higher sensitivity to changes in $N_{tot}$ than to changes in the MSD's shape, except for the case where the MSD contained giant and ultragiant cloud condensation nuclei (GCCN, UGCCN). For increased $N_{tot}$ (for the deep and intermediate profiles), most of the MSDs drove an expected non-monotonic trend of mass and precipitation (the shallow clouds showed only the decreasing part of the curves with mass and precipitation monotonically decreasing). The addition of GCCN and UGCCN drastically changed the non-monotonic trend, such that surface rain saturated and the mass monotonically increased with $N_{tot}$. GCCN and UGCCN changed the interplay between the microphysical processes by triggering an early initiation of collision-coalescence. The early fall-out of drizzle in those cases enhanced the evaporation below the cloud base. Testing the sensitivity of rain yield to GCCN and UGCCN revealed an enhancement of surface rain upon the addition of larger particles to the MSD, up to a certain particle size, when the addition of larger particles resulted in rain suppression. This finding suggests a physical lower bound can be defined for the size ranges of GCCN and UGCCN.



## 1 Introduction

Clouds play a key role in the Earth's climate system. By scattering and absorbing solar and terrestrial radiation, clouds influence the radiative balance. Aerosols influence cloud processes by serving as cloud condensation nuclei (CCN) on which cloud droplets can form (Köhler, 1936). The size of CCN determines the droplets' initial size distribution and hence impacts cloud processes and properties, such as size (Rosenfeld et al., 2008; Altaratz et al., 2014; Koren et al., 2014), lifetime (Albrecht, 1989), optical properties (Twomey and Squires, 1959; Twomey, 1977; Mülmenstädt and Feingold, 2018), and rain amounts and patterns (Yin et al., 2000b; Rosenfeld et al., 2006; Xue et al., 2008; Yuan, 2011; Altaratz et al., 2014; Koren et al., 2014; Seigel, 2014).

The study of giant CCN (GCCN) and ultragiant CCN (UGCCN) and their effects on warm clouds and precipitation have been the subject of various works (Beard and Ochs III, 1993; Feingold et al., 1999; Khain et al., 2000; Yin et al., 2000b; Dagan et al., 2015a). Their size definition is loose, as the lower threshold of GCCN has been defined within a wide range of mean particle diameter ($D_p$) of $2-10\,\mu m$ (Feingold et al., 1999; Yin et al., 2000a), while particles with $D_p > 20\,\mu m$ are usually defined as UGCCN (Feingold et al., 1999; Posselt et al., 2008). Although their observed concentration is low ($< 0.1\,cm^{-3}$; Exton et al., 1986; Flores et al., 2020) in comparison to a typical marine CCN concentration ($50-250\,cm^{-3}$), they have been shown to affect cloud properties, and might even transform non-precipitating clouds to a precipitating state (Feingold et al., 1999).

GCCN and UGCCN stem from a variety of sources, but are considered to be mainly sea-salt (Schulz et al., 2004) and mineral dust (Levin et al., 1996; Tegen et al., 2002). Despite their large size, these particles can be transported thousands of kilometers from their origin. Ultragiant mineral dust particles ($D_p > 75\,\mu m$) have been observed as far as $10,000\,km$ from their origin (Betzer et al., 1988). Other studies have shown even bigger dust particles ($D_p > 200\,\mu m$) carried from Asia to the remote Pacific Ocean, and from the Sahara to Europe (Middleton et al., 2001). Recently, gigantic Saharan dust particles ($D_p \sim 450\,\mu m$) were observed above the Atlantic Ocean $\sim 3,500\,km$ west of the African coast (van der Does et al., 2018).

Aerosols' ability to act as CCN is largely controlled by their size (Dusek et al., 2006), thus, even though mineral dust is less soluble than sea-salt (Petters and Kreidenweis, 2007; Kumar et al., 2009), large mineral dust particles are still considered to act as effective GCCN (Johnson, 1982; Levin et al., 1996; Nenes et al., 2014).

The effect of GCCN and UGCCN on warm clouds' processes is highly important but not fully understood. Early work demonstrated that a few activated UGCCN, and even GCCN (from $\sim 10^{-3}\,cm^{-3}$) can drive early initiation of precipitation, by producing a tail of large drops in the droplet distribution (Johnson, 1982). More recent studies have shown that the effect of GCCN and UGCCN on warm clouds and precipitation is more complex and greatly depends on aerosol concentration. For low aerosol concentration, the addition of GCCN was shown to have little or no effect on precipitation (Teller and Levin, 2006; Zhang et al., 2006; Cheng et al., 2009; Dagan et al., 2015a), due to the early initiation of collision-coalescence and lower supersaturation values (Zhang et al., 2006). In contrast, their effect under polluted conditions is still under debate. It is accepted that the addition of small CCN (for constant liquid water content) leads to the formation of a greater number of smaller droplets, and results in delayed collision-coalescence and a less efficient collection process (Gunn and Phillips, 1957; Squires, 1958; Warner, 1968; Albrecht, 1989). However, addition of GCCN and UGCCN, on one side, has been shown to counteract this delay and act to precede and enhance the collection process, leading to earlier initiation of precipitation (Johnson, 1982; Teller and Levin, 2006; Feingold et al., 1999; Yin et al., 2000b; Rosenfeld et al., 2002; Zhang et al., 2006; Cheng et al., 2009; Dagan et al., 2015a). This was demonstrated for warm convective clouds (Cheng et al., 2009; Dagan et al., 2015a) and stratiform clouds (Feingold et al., 1999; Zhang et al., 2006). On the other side, Khain et al. (2000) reported that the role of GCCN and

UGCCN, though it can be important, is unlikely to be the dominant mechanism of raindrop formation in warm clouds. On a global scale, by using the ECHAM5 General Circulation Model, Posselt et al. (2008) found that adding GCCN induces faster precipitation in warm clouds, and shorter residence times and less accumulation of water in the atmosphere (i.e., accelerating the hydrological cycle).

Here we present a theoretical study, combining new *in-situ* measurements of marine aerosol size distributions (MSD), taken during the *Tara* Pacific expedition (Flores et al., 2020), and a "toy-model" with a detailed description of cloud microphysical processes, to examine the link between MSD and cloud processes and properties (like cloud mass and amount of precipitation), on a single-cloud scale. By using a simplified model, we gain the ability to distill the MSD effect on the interplay between the cloud microphysical processes. This study can be viewed as a basis for a future investigation of this effect on a cloud field scale.

## 2 Methods

### 2.1 MSD Measurements

MSDs were measured aboard the schooner *Tara* over the Atlantic Ocean, Caribbean Sea, and Pacific Ocean during the *Tara* Pacific Expedition (2016–2018). The *Tara* Pacific Expedition primary focus was coral reef research (Planes et al., 2019) with the supporting measurements of discrete surface ocean measurements (Gorsky et al., 2019), and the innovative addition of marine aerosol measurements (Flores et al., 2020). Using a scanning mobility particle sizer (SMPS) in parallel with an optical particle counter (OPC), particles between $0.03 - 32\,\mu m$ (dry diameter) were measured at $\sim 15\,m$ above sea level (ASL) in the Atlantic Ocean and at $\sim 27\,m$ ASL in the Caribbean Sea and western Pacific Ocean (Fig. 1). A Nafion dryer was installed before the SMPS-OPC, which reduced the sampled air relative humidity ($RH$) to below $\sim 35\%$, below the efflorescence point for NaCl (Gupta et al., 2015), thus we considered $D_p$ as dry. The OPC size distributions were corrected and merged with the SMPS size distributions following the method described by Hand and Kreidenweis (2002). For a more detailed description of the aerosol measurements see Flores et al. (2020). Six MSDs were chosen for this study to initiate the cloud simulations (Fig. 1b): two from the Atlantic Ocean, one from the Caribbean Sea, and three from the Pacific Ocean.

The MSDs represent a variety of marine environments with different scenarios: *Atlantic–1*, anthropogenically influenced, with a single mode located between the Aitken and Accumulation modes, highly pronounced coarse and giant modes, and total aerosol concentration ($N_{tot}$) of $2629\,cm^{-3}$; *Atlantic–2*, with comparable Aitken and Accumulation modes, pronounced coarse mode, and no giant mode ($N_{tot} = 416\,cm^{-3}$); *Caribbean–3*, with comparable Aitken and Accumulation modes, a less pronounced coarse mode, and no giant mode ($N_{tot} = 677\,cm^{-3}$); *Pacific–4*, anthropogenically influenced single mode, a less pronounced coarse mode, and no giant mode ($N_{tot} = 4193\,cm^{-3}$); *Pacific–5*, clean marine with a more pronounced Accumulation mode, a diminished coarse mode, and no giant mode ($N_{tot} = 168\,cm^{-3}$); and *Pacific–6*, super clean marine with a more pronounced Aitken mode, a diminished coarse mode, and no giant mode ($N_{tot} = 89\,cm^{-3}$).

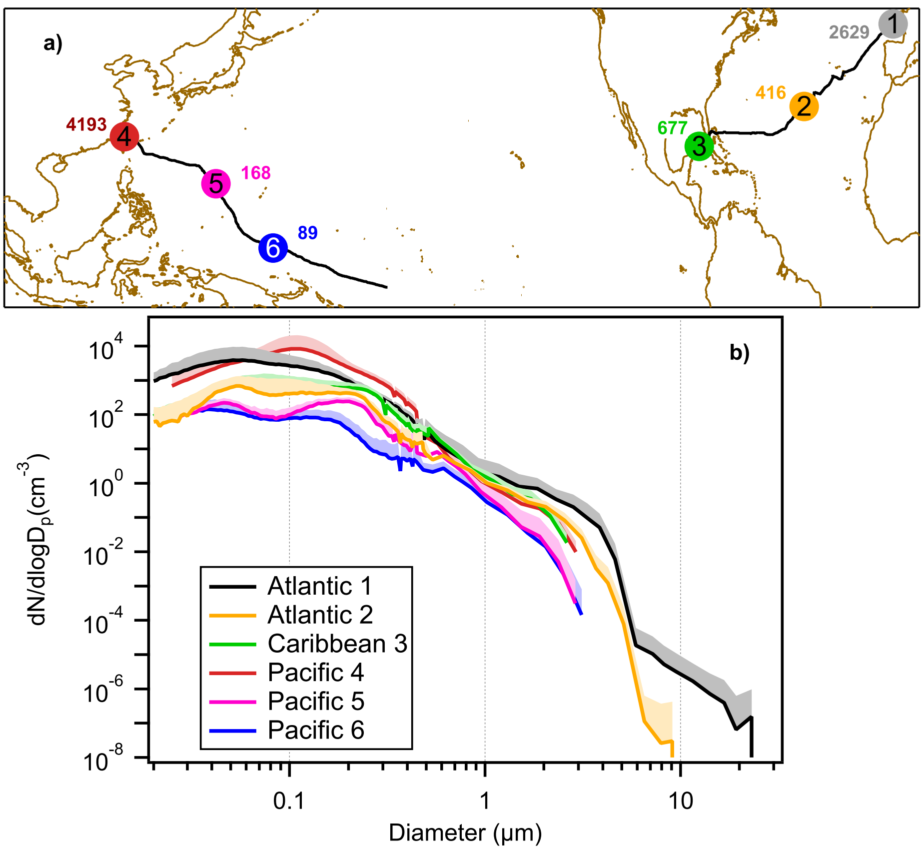


**Figure 1.** (a) *Tara*'s route across the Atlantic Ocean, Caribbean Sea and the Pacific Ocean. Circles indicate the locations of the MSDs used in this study, with total number concentrations written next to each circle. (b) All MSDs; shaded areas represent the upper standard deviation. Each colored curve in (b) is associated with a specific location and total concentration marked in the same color in (a). Each MSD is an average of at least eight hours of measurements.

## 2.2 Model Description and Setup

The Tel-Aviv University axi-symmetric (1.5 D; vertical and radial directions) non-hydrostatic cloud model (TAU–CM) with a detailed cloud microphysics scheme was used (Tzivion et al., 1994; Reisin et al., 1996). The TAU-CM includes warm microphysical processes such as nucleation of CCN, condensation and evaporation, collision-coalescence, breakup (McTaggart-Cowan and List, 1975; Low and List, 1982), and sedimentation (cold processes were excluded here). The microphysical processes are formulated and solved using a multi-moment bin method (Tzivion et al., 1987). CCN of a certain size are activated if the critical supersaturation is reached according to the Köhler equation (Pruppacher and Klett, 1980), taking into account both the curvature and chemical (i.e., solute) effects. All the MSDs were considered to be composed of sea-salt aerosols. To test the sensitivity of the results to different chemical composition, we ran extra simulations changing the aerosol's composition to ammonium sulfate, and found no substantial differences.

The model was run at $50\,m$ resolution in the vertical and horizontal directions, and a temporal resolution of $1\,s$. The model was initialized using three idealized atmospheric profiles. We chose to use the idealized profiles since the MSDs were sampled throughout different places (see Fig. 1), and our focus is on the MSD's effect. The profiles represent a relatively moist tropical environment (Garstang and Betts, 1974; Dagan et al., 2015b), but differ in the inversion layer height and $RH$ in the cloudy layer, resulting in a shallow, intermediate, and deeper cloudy layers. The deepest profile included a well-mixed sub-cloud layer between $0-1000\,m$, and a conditionally unstable cloudy layer between $1000$ and $4000\,m$ ($3000$, $2000\,m$ for the other profiles) with an $RH$ of 95% (90, 80%). The cloudy layers were bounded by an overlying inversion layer with a temperature gradient of $2^o$C over $50\,m$, and $RH$ of 30%. Here we focus on the deepest profile (highest inversion height and $RH$), and present some of the results from the shallow and intermediate profiles in the supplementary information (SI). This choice was made because a larger aerosol concentration optimum is expected for larger clouds (Dagan et al., 2015b). This allowed us to examine the full effect of the different MSDs on cloud microphysical processes. Each of the six MSDs was normalized to the five other MSD concentrations, to preserve the original shape (see Fig. S1; total of 36 MSDs and 108 simulations for three initialization profiles). As we normalized the MSDs to higher values of $N_{tot}$, the MSDs shifted such that they contained larger particles (Fig. S1). However, only the *Atlantic—1* and *Atlantic–2* MSDs contained GCCN, and the *Atlantic–1* was the only MSD that contained UGCCN even in the case of the highest aerosol concentration.

## 3 Results and Discussion

First, we explored the link between the MSD and the cloud's bulk properties (total mass and rain yield) as a function of the total aerosol concentration ($N_{tot}$).

Figure 2 shows the total accumulated rain yield at the surface (Fig. 2a) and the maximum cloud mass for each simulation (Fig. 2b) as a function of the $N_{tot}$ used in that simulation. Each curve presents the results of six different simulations conducted using the same MSD shape but with different concentration (each MSD was normalized to the concentration of the other MSDs while maintaining its shape). As can be seen in Fig. 2 (and in Fig. S2 for the two other atmospheric profiles), the *Atlantic–1*

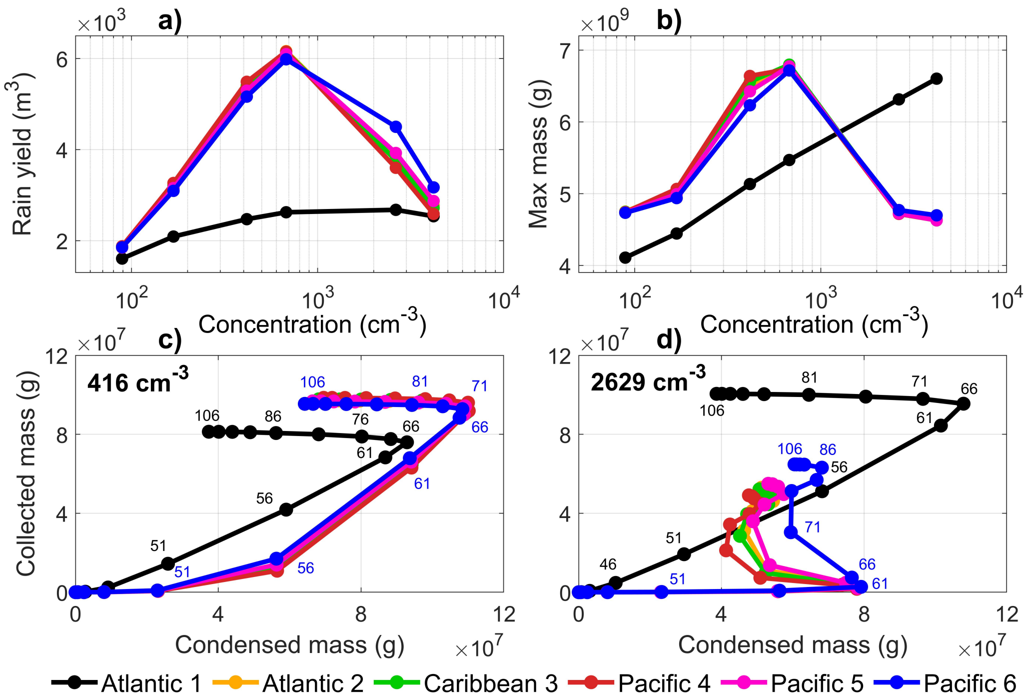


**Figure 2.** (a) Surface rain yield and (b) cloud's maximum mass as a function of $N_{tot}$ used in the simulation, integrated over 150 minutes of simulations. Each curve represents six simulations, done with a specific shape of the MSD normalized to different aerosol concentrations. The lower panels (c, d) show the time evolution of accumulated condensed mass versus accumulated collected mass. The simulated time is noted along the black and blue curves for the *Atlantic–1* and *Pacific–6* MSDs, respectively. The panels represent an aerosol concentration of 416 and 2629 $cm^{-3}$ (c and d, respectively).

clouds have a distinct curve compared to the rest of the MSDs for all profiles. We will first describe the curves of the other five MSD clouds, and later focus on the exceptional *Atlantic–1* curve and its driving mechanisms.

The general shape of the five curves is similar for the deep and intermediate profiles, and exhibits a non-monotonic trend (see Fig. 2a–b and Fig. S2a–b, respectively): an increase in total rain yield and the cloud's maximum mass as a function of aerosol loading, up to a maximum optimal aerosol concentration ($N_{op}$), followed by a decrease. All five curves have a similar $N_{op}$ of around $N_{tot} = 677\,cm^{-3}$ ($N_{tot} = 416\,cm^{-3}$ for the intermediate profile) for both surface rain yield and maximum cloud mass. For the shallow profile, the five MSD curves preset only the decreasing branch, with a minor decrease in rain yield and cloud mass with increasing aerosol loading. The non-monotonic trend can be explained by the interaction of competing processes (Dagan et al., 2015b). The ascending branch (moving from extremely clean to slightly polluted conditions) can be explained by the increased droplets surface area, which enhances condensation efficiency (Pinsky et al., 2013; Seiki and Nakajima, 2014) and delays the initiation of collision-coalescence (see Fig. S3a–b). The delayed initiation of collision-coalescence drives longer condensational growth (hence, latent heat release also increases), and the droplets reach higher in the atmosphere (larger droplet mobility; Koren et al. (2015)). This chain of processes drives deeper clouds with more liquid mass (i.e., cloud invigoration). On the other hand, the descending branch ($N_{tot} > N_{op}$) is caused by enhanced periphery processes, entrainment and evaporation, which take over and result in cloud suppression (see evaporation in Fig. S3c and Dagan et al. (2015b)). The value of $N_{op}$ depends on the atmospheric profile (Dagan et al., 2015b), such that it decreases as the profile becomes shallower (i.e., lower inversion base and $RH$; Fig. S2). For the cases of shallower cloudy–layers, where the clouds are more subjected to entrainment effects, the ascending branch of the curves is less pronounced (intermediate profile, Fig. S2a–b) or non-existent (shallow profile, Fig. S2c–d). We, therefore, focus on the deepest atmospheric profile, which better demonstrates the full effect of the competition and interactions between the microphysical processes in the clouds, and refer to Text S2 in the SI for the intermediate and shallow profiles.

The curve formed by the *Atlantic–1* MSD clouds (black line in Fig. 2) is dramatically different from the other five curves. It shows not only significantly lower values for most of the simulations (except for the cloud mass for $N_{tot} > \sim 1000\,cm^{-3}$), but also different trends in both rain yield and cloud mass. For $N_{tot} < 1000\,cm^{-3}$, the trends of both surface rain and the cloud's maximum mass show an increase with increasing aerosol loading, similar to the other five MSD curves. However, for higher values of aerosol concentration, the rain yield saturates, and the cloud's maximum mass continues to increase with no $N_{op}$ (for higher aerosol concentration values, see Fig. S4).

The flattening of the rain yield curve is attributed to the presence of GCCN (Dagan et al., 2015a). The *Atlantic–1* MSD has three distinct modes: one influenced by pollution, one of coarse particles, and one of GCCN. Next, we examined how the coarse and giant modes, which are by far more pronounced in the *Atlantic–1* MSD than in the other five MSDs, account for the unique behavior of these clouds.

To explore the *Atlantic–1* MSD monotonic increase in maximum cloud mass with $N_{tot}$, we examined the time evolution of the cloud's microphysical processes. Figure 2c–d shows the evolution of the six cloud trajectories on the phase space spanned by the accumulated condensed mass (representing droplet nucleation and condensational growth) and the accumulated collected mass (representing the collision-coalescence processes), for a medium aerosol concentration level ($N_{tot}$ normalized to $416\,cm^{-3}$, Fig. 2c) and a more polluted one ($N_{tot}$ normalized to $2629\,cm^{-3}$, Fig. 2d). Note that the collected mass represents an internal redistribution of the liquid water mass with no change in the total mass. For the cleaner cases, where the aerosol loading is a bit lower than $N_{op}$, in the first stage, all but the *Atlantic–1* clouds, accumulate mass by nucleation and condensation without any contribution from the collection process. At a later stage in the cloud's lifetime, the trajectories turn diagonally up ($\sim$56 $min$ into the simulation), showing that the collection process has begun. Finally, the clouds stop growing by condensation, reaching their maximum mass, and begin to evaporate ($\sim$71 $min$ into the simulation; trajectories turn to the left). In the *Atlantic–1* MSD case, the collection process kicks in earlier, within 10 minutes of the cloud's lifetime ($\sim$51 $min$ into the simulation), due to the presence of GCCN in the MSD which initially form bigger droplets. The bigger droplets formed by the nucleation of GCCN resulted in a lower droplets' surface area for a given total water mass (compared to the one that would have formed from droplets nucleated on smaller CCNs) for the *Atlantic–1* MSD case compared with the other MSDs (Fig. S5). The lower total droplets' surface area was then further reduced by the early initiation of the collection process. Moreover, these bigger droplets rapidly grow into drizzle-sized drops and sediment out of the cloud, accounting for the smaller maximum condensed mass in the *Atlantic–1* case compared to the other five cases.

Under more polluted conditions, the trajectory of the *Atlantic–1* MSD cloud (black curve in Fig. 2d) on this phase space is similar (in shape) to the one in the cleaner case (black curve in Fig. 2c), but this cloud accumulates more mass, due to the larger droplet surface area (Fig. S5b–c). However, the *Atlantic—1*'s total droplet surface area is lower in comparison to the rest of the clouds (Fig. S5c), and still, it condenses more mass, reaching $\sim 11 \times 10^7 g$ compared to $\sim 8 \times 10^7 g$ as the rest of the clouds. This can be explained by the nucleation of the GCCN and UGCCN that are present in the *Atlantic–1* MSD under polluted conditions, which on the one hand, accumulate more mass (Fig. 2d) and drive a significantly higher number of raindrops at the growing stage of the cloud (Fig. S8), and on the other hand, results in a lower droplet number concentration ($N_d$) compared to the other clouds (Fig. S7). Therefore, the vertical distribution of mass of the *Atlantic–1* cloud is dominated by the precipitating particles, unlike the other clouds (Figs. S7 and S8). Note that while the total cloud mass of the *Atlantic–1* is larger than the one obtained by the other clouds, it is in the same order of magnitude. However, the mass of precipitating particles in the *Atlantic–1* cloud overwhelms the ones exhibited by the other MSDs. Contrastingly, the $N_d$ of the other clouds is much higher than the one of the *Atlantic–1* cloud, allowing for collision-coalescence to begin toward the end of the condensational growth stage, or after the evaporation process has begun (e.g., *Pacific–4*, the trajectories turn back to the left before acquiring a vertical component), and to increase in a slow pace. For the *Atlantic–1* cloud, the accumulation of liquid water by nucleation and condensation occurs in parallel to the collection process that starts much earlier in this case (Fig. 2d). The timing of the initiation of collision-coalescence further explains the decreasing branch of the rain yield trend for all MSDs aside from *Atlantic–1* (Fig. 2a), as it starts too late in the cloud's lifetime (after the cloud has already begun to lose mass).

This, however, does not explain the overall smaller surface rain yield of the *Atlantic–1* MSD clouds for all aerosol concentrations, nor the saturation trend for high $N_{tot}$ (Fig. 2a). To further inspect the lower surface rain yield, we examined the temporal evolution of evaporation below the cloud base, and the surface rain rate for the different MSD clouds. Figure 3 shows the evaporation below the cloud base (left column), and the surface rain rate (right column) as a function of time for four different $N_{tot}$ ($89, 416, 2629, 4193\, cm^{-3}$ – from upper to lower panels).

Two main features can be seen for the *Atlantic–1* case regardless of $N_{tot}$: (i) both evaporation below the cloud base and surface rain start earlier than in the rest of the cases. This is due to the early onset of collision-coalescence (Fig. 2c–d), which converts the already big particles into drizzle-sized drops; (ii) evaporation below cloud base is always larger and, at the same time, the surface rain rate is lower. However, the magnitude of both evaporation below the cloud base and surface rain rate does depend on $N_{tot}$, ranging from $0.17 - 2.16 \times 10^7\, g\, s^{-1}$ and $0.42 - 4.76 \times 10^7\, g\, s^{-1}$, respectively.

The smaller values of the surface rain yield for the *Atlantic–1* MSD, and the non-monotonic trend for the rest of the MSDs (Fig. 2a), are also evident in the temporal evolution of surface rain rate (right column of Fig. 3). Part of this is explained above, by the interplay between different internal cloud processes, but it does not elucidate the complete mechanism. Figure 3 shows that evaporation below the cloud base plays a crucial role in determining the low values of the surface rain in the *Atlantic–1* case. As $N_{tot}$ increases, more GCCN are present (Fig. S1) and preferentially activated, growing rapidly into drizzle-sized drops (see Fig. S8), which immediately begin to precipitate. This reduces their time spent in the cloud, and they are thus large enough to fall, but still too small to reach the surface before they fully evaporate. The *Atlantic–1* raindrops are considerably smaller than those produced by the other clouds (Fig. S6), and their evaporation is therefore more efficient. Moreover, the rain falls

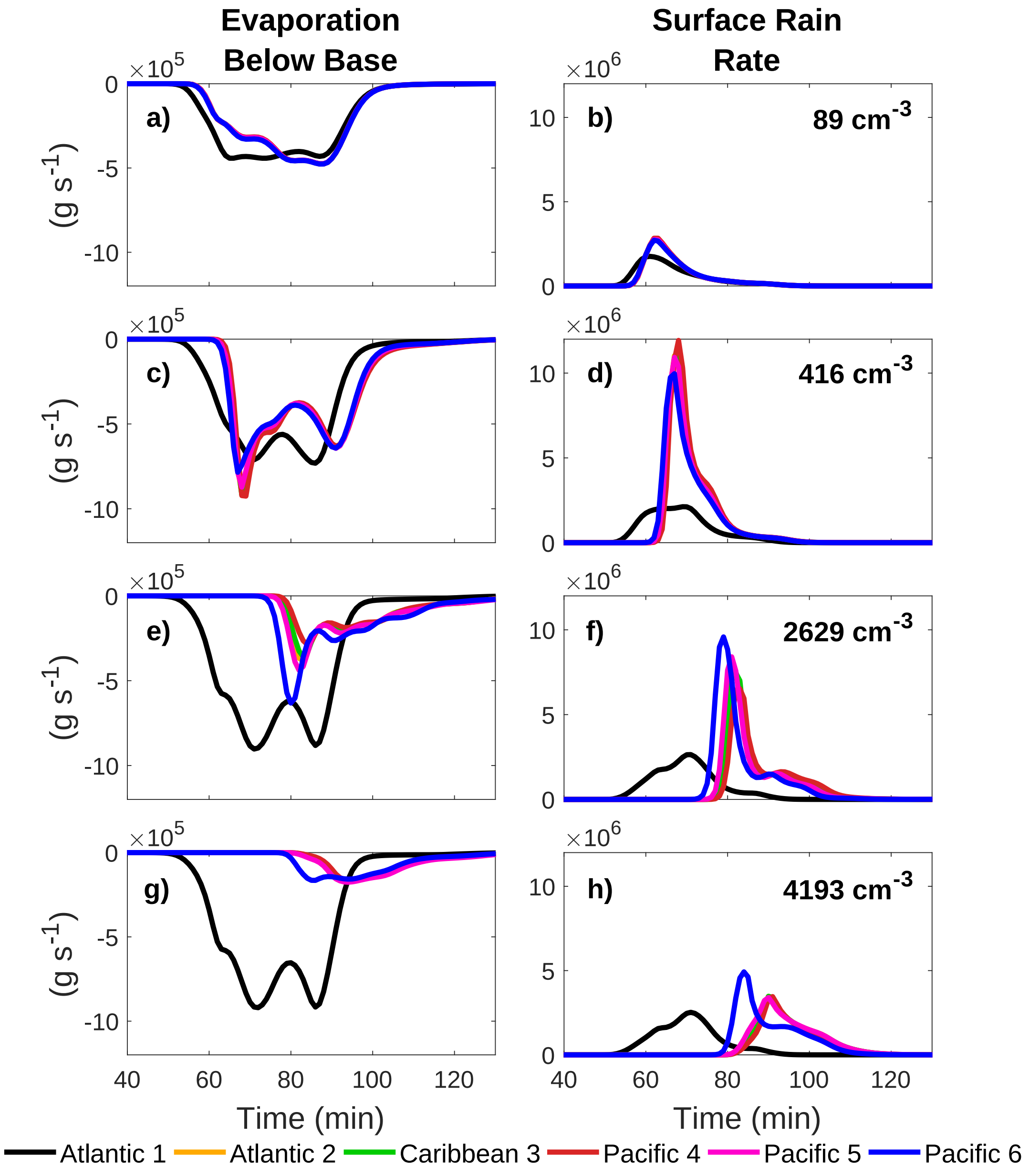


**Figure 3.** Time evolution of the evaporated mass below the cloud base and surface rain mass per unit time (left and right columns, respectively). Each row represents a specific $N_{tot}$: $89\,cm^{-3}$(a, b), $416\,cm^{-3}$ (c, d), $2629\,cm^{-3}$ (e, f), and $4193\,cm^{-3}$ (g, h), as shown in the upper right corner of each row. The different curves in each panel represent an MSD shape normalized to the specific $N_{tot}$. Note that there is an order of magnitude difference between the exponent in the right and left columns.

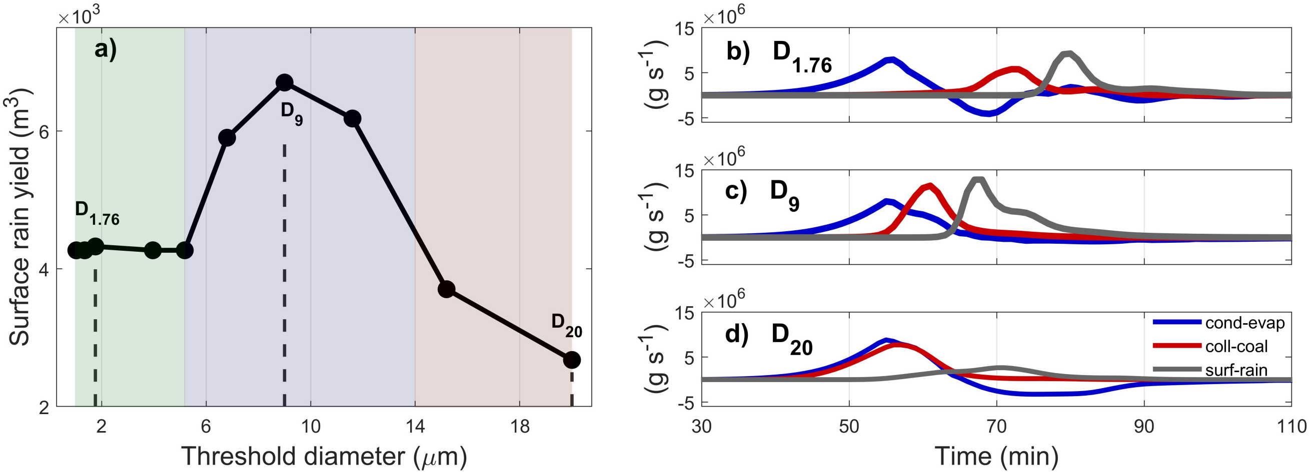


**Figure 4.** (a) Surface rain yield ($m^3$) as a function of a threshold diameter (no particles bigger than that diameter) for the *Atlantic–1* MSD. Each circle in (a) represents a subtraction of specific bins from the MSD. The shaded areas indicate the different trends of the curve. (b–d) Condensed–evaporated mass (blue), collected mass (red), and surface rain rate (gray) per unit time, as a function of time for selected threshold diameters matching three simulations from (a). The specific threshold diameters are marked in the upper left corner of each panel ($D_{1.76}$, $D_9$, and $D_{20}\,\mu m$: b-d, respectively), and (d) represents the full *Atlantic–1* MSD.

below the cloud base earlier, compared to the other MSDs cases, while the cloud is still in its developing stage, meaning that the cloud and the sub—cloud layers are dominated by updrafts, and the sub–cloud layer is consequently drier (Fig. S7). The combination of the small raindrops with their early fall out that lasts longer (due to the updrafts prevailing at this stage) results in greater rain evaporation below the cloud base for the *Atlantic—1* MSD. A more substantial evaporation below the cloud base can lead to a larger descent of cold air to the surface and eventually, to cold pool formation, which affects cloud field organization (Warner et al., 1979; Zuidema et al., 2012; Seifert and Heus, 2013; Dagan et al., 2018).

Finally, to ensure that this reported effect is indeed a direct result of the presence of GCCN and UGCCN, we investigated the impact of the different parts of the *Atlantic–1* MSD on cloud processes. We performed additional sensitivity simulations using the *Atlantic–1* MSD in which the largest aerosol size bins were gradually excluded from the distribution. This resulted in a very minor change in $N_{tot}$ ($< 0.001\%$), due to the small number concentration of the excluded large particles.

Figure 4a shows the total surface rain yield for a specific simulation as a function of the aerosol threshold diameter used in that simulation (above which the particle concentration was set to zero). For example, $D_9$ represents a simulation in which the *Atlantic–1* MSD was truncated at an aerosol diameter of $9\,\mu m$ (i.e., all size bins with diameters larger than this threshold were set to zero). The behavior of the surface rain yield as a function of threshold diameter revealed that the amount of precipitation reaching the surface is highly dependent on the existence of GCCN and UGCCN, and more specifically on their sizes. The curve shows a non-monotonic trend that starts with a plateau, where the addition of larger particles (increase in threshold diameter) does not affect the surface precipitation ($D_{1.03} - D_{5.81}$, green shading). This stable behavior is followed by a range of sizes where the addition of particles results in an enhanced amount of surface rain ($D_{5.81}- \sim D_{14}$, blue shading). The maximum surface rain yield ($6.7 \times 10^3\, m^3$) is obtained at an optimum threshold diameter ($D_{op}$) of $\sim 9\, \mu m$. As particles greater than $\sim$14 $\mu m$ in diameter were included in the MSD, the rain yields decreased below the mean values of the plateau ($D_{14}- \sim D_{20}$, red shading). The changing trends of the curve suggest that the thresholds used to define GCCN and UGCCN can be taken from a more physical source, rather than a loose definition. We propose that the threshold diameter for which the surface rain yield is enhanced be defined as the lower bound for GCCN, and the threshold diameter for which surface rain begins to be suppressed as the lower bound for UGCCN. For this study, using the *Atlantic–1* MSD and the specific atmospheric conditions (described in section 2.2), the lower bound of GCCN is $D_p \cong 5 \mu m$, and for UGCCN $D_p \cong 14\, \mu m$.

Figure 4b–d shows the evolution (timing and magnitude) of the condensation–evaporation processes (nucleation and diffusional growth), collision-coalescence, and surface rain rate for three selected threshold diameters ($D_{1.76}$, $D_9$ and $D_{20}$). It sheds light on the different trends shown in Figure 4a. The larger the particles in the MSD, the faster the critical size for the initiation of the collision-coalescence process is reached, and the sooner it occurs. The initiation of collision-coalescence shortens from $\sim$65 minutes of simulation for the $D_{1.76}$ case to $\sim$45 minutes of simulation for the $D_{20}$ case, where it starts almost immediately after condensation begins (Fig. 4b and d, respectively).

For optimal rain production, collision-coalescence has to be correctly timed with the condensational growth of the cloud (Dagan et al., 2015a). For the $D_{1.76}$ case, collision-coalescence starts only after condensational growth has ceased, and peaks when evaporation is the dominant process ($\sim$62 and $\sim$72 minutes into the simulation, respectively). Whereas, for $D_9$ it starts earlier ($\sim$55 minutes into the simulation) while condensation peaks, and for the $D_{20}$ case (i.e., the full *Atlantic–1* MSD), the peaks of the collision-coalescence and condensation processes occur at nearly the same time ($\sim$56 minutes into the simulation). The optimum threshold diameter dictates the correct timing for the microphysical processes, such that maximum liquid water mass is converted to surface rain. For the *Atlantic–1* MSD (under the deepest atmospheric profile), the maximum surface rain is obtained for $D_{op} \sim 9\, \mu m$ (Fig. 4c).

## 4 Summary

In this study, we used six MSDs measured *in-situ* in the Atlantic Ocean, Caribbean Sea and Pacific Ocean to study the effect of aerosol concentration and size on warm clouds' properties. The MSDs differed in shape and ranged in total aerosol concentration from very clean ($89\, cm^{-3}$, *Pacific–6*) to polluted ($4193\, cm^{-3}$, *Pacific–4*) conditions. By equating the $N_{tot}$ of the different MSDs (i.e., normalizing them to match the six specific $N_{tot}$) we altered their total aerosol concentration, while keeping the amount of small versus big aerosols constant. This affected the initial droplet size distributions in terms of the total number of droplets, and the droplets' sizes.

Using an axisymmetric cloud model with detailed bin–microphysics, we examined the sensitivity of key properties of warm clouds (cloud maximum mass and surface rain) to the measured MSDs on a single cloud scale, under a range of environmental conditions (going from shallow to intermediate and deeper conditions, using three atmospheric profiles). We focused on the deepest profile, since it best captured the effect of competing microphysical cloud processes, and showed that surface rain yield and cloud's maximum mass are affected in a non-monotonic way by changes in $N_{tot}$, and the shape of the MSDs for most of the cases. This was also the case for the intermediate profile results, while the shallow one only showed the decreasing branch of this non-monotonic trend, due to more dominant entrainment effects.

All MSD shapes, except for the *Atlantic–1*, shared a similar trend as a function of $N_{tot}$, starting with an increase in cloud mass and surface rain yield up to an $N_{op}$ of $\sim 700\,cm^{-3}$, followed by a decrease for higher aerosol loading. This consistent behavior was altered by the increased concentration of giant particles in the *Atlantic–1* MSD. Namely, the maximum cloud mass monotonically increased as a function of $N_{tot}$, while the surface rain yield also increased but then saturated at high aerosol concentrations (with no $N_{op}$). The surface rain yield also had lower values in all cases, dropping by a factor of up to 2.3. The former can be explained by efficient nucleation of the big aerosols, and the latter can be explained by the initiation time of collision-coalescence with respect to the optimal timing for accumulation of enough water by condensation, enabling more water to become available for rain production.

In addition, the immediate sedimentation post-nucleation produced small raindrops that fall early, but evaporate below the cloud base before they reach the surface. Although the MSDs differed throughout the entire spectrum of aerosol sizes, this study shows that it is the existence of the giant mode that dramatically changes cloud properties, especially with respect to surface precipitation.

A deeper investigation of the effect of GCCN and UGCCN was preformed by gradually eliminating the largest particles from the *Atlantic–1* MSD. We found that above a threshold diameter of $\sim 5\,\mu m$, collision-coalescence begins earlier, such that the surface rain is enhanced. This behavior is disrupted when the threshold diameter reaches $\sim 14\,\mu m$, with a further increase in threshold diameter resulting in lower surface rain yield. The rain suppression observed from this threshold diameter on is explained by the dramatically reduced droplet surface area, and the initiation of collision-coalescence at a much earlier stage. This results in the fast formation of large drops and the early fall-out of drizzle while the cloud is still in its developing stage, such that updrafts prevail and the sub–cloud layer is drier. The combination of a sub–cloud layer that is dominated by updrafts and features lower $RH$ values, further promotes longer fall time for the small raindrops and an efficient evaporation below the *Atlantic—1* cloud base. These two values of threshold diameter are suggested to define the lower bounds of GCCN and UGCCN. They depend on specific conditions, such as the atmospheric profile, $N_{tot}$ and the shape of the aerosol size distribution.

The *Atlantic–1* MSD was measured off the coast of France (see Fig. 1a). Scanning electron microscope images of the aerosols collected during the same time period highlight the differences between the particles. From a giant mode comprised of $\sim 1\,\mu m$ Brochosomes-like particles (Fig. 5a), to an ultragiant mode comprised of $\sim 20\,\mu m$ mineral dust particles (Fig. 5b).

Here, we considered only changes in $N_{tot}$ and the MSD's shape. In addition, we also examined the sensitivity of the results to different chemical composition, which in the TAU–CM model affected the Köhler activation. Future work is needed to further explore how the chemical composition of the particles affects warm cloud's properties.

This study demonstrates the importance of the aerosol size distribution in terms of both total number concentration and the aerosol distribution shape, which can impact cloud properties. Currently, most aerosol measurements restrict the upper limit of particle sizes to $D_p = 10\,\mu m$ (i.e., $PM_{10}$). Consequently, most of the cloud-resolving models, even those using bin-

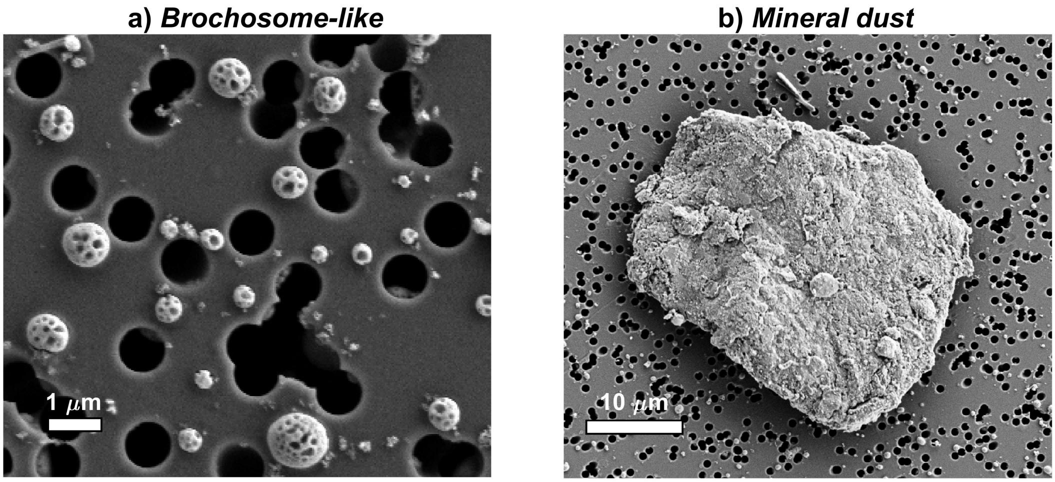


**Figure 5.** Scanning electron microscope images of Brochosome–like particles (a), and mineral dust (b) collected during the same period as the *Atlantic–1* MSD measurement.

microphysics, do not allow for ultragiant or even giant particles. Many of these models use a "typical" 'wide-marine' or 'narrow-continental' size distribution that does not account for the natural variability in aerosol size distributions or reflect their complexity. Additionally, with the mounting evidence of microplastic particles, with sizes between $4-188\,\mu m$, present in the atmosphere and in rain (Allen et al., 2020; Brahney et al., 2020), it is of greater importance to include and further study the impact of particles with $D_p > 10\,\mu m$ on cloud and precipitation.

*Data availability.* Key parameters from this study are included in the SI, and will be uploaded to a public repository.

*Author contributions.* J.M.F and G.D conceived the presented idea. T.D. lead the simulations and G.D. supported. J.M.F. performed the measurements. All authors provided critical feedback and helped shape the research, analysis and manuscript. T.D. and J.M.F. took the lead in writing the manuscript, and contributed equally to this manuscript.

*Competing interests.* The authors declare no competing interests.

*Acknowledgements.* This research was partially supported by a research grant from Scott Jordan and Gina Valdez, the De-Botton center for Marine Science, the Yeda-Sela center for basic research, and a research grant from the Yotam project.
We are keen to thank the following institutions for their financial and scientific support that made the unique *Tara* Pacific expedition possible:

CNRS, PSL, CSM, EPHE, Genoscope/CEA, ANR, agnes b., the Veolia Foundation, Region Bretagne, Billerudkorsnas, Amerisource Bergen Company, Altran, Lorient Agglomeration, Prince Albert II de Monaco Foundation, L'Oreal, Biotherm, France Collectivites, FFEM, the Tara Foundation teams, crew and board members. Tara Pacific would not exist without the continuous support of the participating institutes. The authors also particularly thank Serge Planes, Denis Allemand and the Tara Pacific consortium. This is publication number 14 of the Tara Pacific Consortium.

## References


Albrecht, B. A.: Aerosols, cloud microphysics, and fractional cloudiness, Science, 245, 1227–1230, 1989.

Allen, S., Allen, D., Moss, K., Le Roux, G., Phoenix, V. R., and Sonke, J. E.: Examination of the ocean as a source for atmospheric microplastics, PloS one, 15, e0232 746, 2020.

Altaratz, O., Koren, I., Remer, L., and Hirsch, E.: Cloud invigoration by aerosols—Coupling between microphysics and dynamics, Atmospheric Research, 140, 38–60, 2014.

Beard, K. V. and Ochs III, H. T.: Warm-rain initiation: An overview of microphysical mechanisms, Journal of Applied Meteorology, 32, 608–625, 1993.

Betzer, P., Carder, K., Duce, R., Merrill, J., Tindale, N., Uematsu, M., Costello, D., Young, R., Feely, R., Breland, J., et al.: Long–range transport of giant mineral aerosol particles, Nature, 336, 568, 1988.

Brahney, J., Hallerud, M., Heim, E., Hahnenberger, M., and Sukumaran, S.: Plastic rain in protected areas of the United States, Science, 368, 1257–1260, 2020.

Cheng, W. Y., Carrió, G. G., Cotton, W. R., and Saleeby, S. M.: Influence of cloud condensation and giant cloud condensation nuclei on the development of precipitating trade wind cumuli in a large eddy simulation, Journal of Geophysical Research: Atmospheres, 114, 2009.

Dagan, G., Koren, I., and Altaratz, O.: Aerosol effects on the timing of warm rain processes, Geophysical Research Letters, 42, 4590–4598, 2015a.

Dagan, G., Koren, I., and Altaratz, O.: Competition between core and periphery-based processes in warm convective clouds–from invigoration to suppression, Atmospheric Chemistry and Physics, 15, 2749–2760, 2015b.

Dagan, G., Koren, I., Altaratz, O., and Feingold, G.: Feedback mechanisms of shallow convective clouds in a warmer climate as demonstrated by changes in buoyancy, Environmental Research Letters, 13, 054 033, 2018.

Dusek, U., Frank, G., Hildebrandt, L., Curtius, J., Schneider, J., Walter, S., Chand, D., Drewnick, F., Hings, S., Jung, D., et al.: Size matters more than chemistry for cloud-nucleating ability of aerosol particles, Science, 312, 1375–1378, 2006.

Exton, H., Latham, J., Park, P., Smith, M., and Allan, R.: The production and dispersal of maritime aerosol, in: Oceanic Whitecaps, pp. 175–193, Springer, 1986.

Feingold, G., Cotton, W. R., Kreidenweis, S. M., and Davis, J. T.: The impact of giant cloud condensation nuclei on drizzle formation in stratocumulus: Implications for cloud radiative properties, Journal of the atmospheric sciences, 56, 4100–4117, 1999.

Flores, J., Bourdin, G., Altaratz, O., Trainic, M., Lang-Yona, N., Dzimban, E., Steinau, S., Tettich, F., Planes, S., Allemand, D., et al.: Tara Pacific Expedition's Atmospheric Measurements of Marine Aerosols across the Atlantic and Pacific Oceans: Overview and Preliminary Results, Bulletin of the American Meteorological Society, 101, E536–E554, 2020.

Garstang, M. and Betts, A. K.: A review of the tropical boundary layer and cumulus convection: Structure, parameterization, and modeling, Bulletin of the American Meteorological Society, 55, 1195–1205, 1974.

Gorsky, G., Bourdin, G., Lombard, F., Pedrotti, M. L., Audrain, S., Bin, N., Boss, E., Bowler, C., Cassar, N., Caudan, L., et al.: Expanding Tara Oceans protocols for underway, ecosystemic sampling of the ocean-atmosphere interface during Tara Pacific expedition (2016-18), Frontiers in Marine Science, 6, 750, 2019.

Gunn, R. and Phillips, B.: An experimental investigation of the effect of air pollution on the initiation of rain, Journal of Meteorology, 14, 272–280, 1957.

Gupta, D., Kim, H., Park, G., Li, X., Eom, H.-J., and Ro, C.-U.: Hygroscopic properties of NaCl and NaNO 3 mixture particles as reacted inorganic sea-salt aerosol surrogates., Atmospheric Chemistry & Physics, 15, 2015.

Hand, J. L. and Kreidenweis, S. M.: A new method for retrieving particle refractive index and effective density from aerosol size distribution data, Aerosol Science & Technology, 36, 1012–1026, 2002.

Johnson, D. B.: The role of giant and ultragiant aerosol particles in warm rain initiation, Journal of the Atmospheric Sciences, 39, 448–460, 1982.

Khain, A., Ovtchinnikov, M., Pinsky, M., Pokrovsky, A., and Krugliak, H.: Notes on the state-of-the-art numerical modeling of cloud microphysics, Atmospheric Research, 55, 159–224, 2000.

Köhler, H.: The nucleus in and the growth of hygroscopic droplets, Transactions of the Faraday Society, 32, 1152–1161, 1936.

Koren, I., Dagan, G., and Altaratz, O.: From aerosol-limited to invigoration of warm convective clouds, Science, 344, 1143–1146, 2014.

Koren, I., Altaratz, O., and Dagan, G.: Aerosol effect on the mobility of cloud droplets, Environmental Research Letters, 10, 104 011, 2015.

Kumar, P., Nenes, A., and Sokolik, I. N.: Importance of adsorption for CCN activity and hygroscopic properties of mineral dust aerosol, Geophysical Research Letters, 36, 2009.

Levin, Z., Ganor, E., and Gladstein, V.: The effects of desert particles coated with sulfate on rain formation in the eastern Mediterranean, Journal of Applied Meteorology, 35, 1511–1523, 1996.

Low, T. and List, R.: Collision, coalescence and breakup of raindrops. Part II: Parameterization of fragment size distributions, Journal of the Atmospheric Sciences, 39, 1607–1619, 1982.

McTaggart-Cowan, J. D. and List, R.: Collision and breakup of water drops at terminal velocity, Journal of the Atmospheric Sciences, 32, 1401–1411, 1975.

Middleton, N., Betzer, P., and Bull, P.: Long-range transport of ’giant’ aeolian quartz grains: linkage with discrete sedimentary sources and implications for protective particle transfer, Marine Geology, 177, 411–417, 2001.

Mülmenstädt, J. and Feingold, G.: The radiative forcing of aerosol–cloud interactions in liquid clouds: wrestling and embracing uncertainty, Current Climate Change Reports, 4, 23–40, 2018.

Nenes, A., Murray, B., and Bougiatioti, A.: Mineral dust and its microphysical interactions with clouds, in: Mineral Dust, pp. 287–325, Springer, 2014.

Petters, M. and Kreidenweis, S.: A single parameter representation of hygroscopic growth and cloud condensation nucleus activity, Atmospheric Chemistry and Physics, 7, 1961–1971, 2007.

Pinsky, M., Mazin, I., Korolev, A., and Khain, A.: Supersaturation and diffusional droplet growth in liquid clouds, Journal of the Atmospheric Sciences, 70, 2778–2793, 2013.

Planes, S., Allemand, D., Agostini, S., Banaigs, B., Boissin, E., Boss, E., Bourdin, G., Bowler, C., Douville, E., Flores, J. M., et al.: The Tara Pacific expedition—A pan-ecosystemic approach of the “-omics” complexity of coral reef holobionts across the Pacific Ocean, PLoS biology, 17, e3000 483, 2019.

Posselt, D., Van Den Heever, S., and Stephens, G.: Trimodal cloudiness and tropical stable layers in simulations of radiative convective equilibrium, Geophysical Research Letters, 35, 2008.

Pruppacher, H. R. and Klett, J. D.: Microphysics of clouds and precipitation, Nature, 284, 88–88, 1980.

Reisin, T., Levin, Z., and Tzivion, S.: Rain production in convective clouds as simulated in an axisymmetric model with detailed microphysics. Part I: Description of the model, Journal of the atmospheric sciences, 53, 497–519, 1996.

Rosenfeld, D., Lahav, R., Khain, A., and Pinsky, M.: The role of sea spray in cleansing air pollution over ocean via cloud processes, Science, 297, 1667–1670, 2002.

Rosenfeld, D., Kaufman, Y., and Koren, I.: Switching cloud cover and dynamical regimes from open to closed Benard cells in response to the suppression of precipitation by aerosols, Atmospheric Chemistry and Physics, 6, 2503–2511, 2006.

Rosenfeld, D., Lohmann, U., Raga, G. B., O'Dowd, C. D., Kulmala, M., Fuzzi, S., Reissell, A., and Andreae, M. O.: Flood or drought: how do aerosols affect precipitation?, science, 321, 1309–1313, 2008.

Schulz, M., de Leeuw, G., and Balkanski, Y.: Sea-salt aerosol source functions and emissions, in: Emissions of Atmospheric Trace Compounds, pp. 333–359, Springer, 2004.

Seifert, A. and Heus, T.: Large-eddy simulation of organized precipitating trade wind cumulus clouds, Atmos. Chem. Phys, 13, 5631–5645, 2013.

Seigel, R. B.: Shallow cumulus mixing and subcloud-layer responses to variations in aerosol loading, Journal of the Atmospheric Sciences, 71, 2581–2603, 2014.

Seiki, T. and Nakajima, T.: Aerosol effects of the condensation process on a convective cloud simulation, Journal of the Atmospheric Sciences, 71, 833–853, 2014.

Squires, P.: The microstructure and colloidal stability of warm clouds, Tellus, 10, 262–271, 1958.

Tegen, I., Harrison, S. P., Kohfeld, K., Prentice, I. C., Coe, M., and Heimann, M.: Impact of vegetation and preferential source areas on global dust aerosol: Results from a model study, Journal of Geophysical Research: Atmospheres, 107, AAC–14, 2002.

Teller, A. and Levin, Z.: The effects of aerosols on precipitation and dimensions of subtropical clouds: a sensitivity study using a numerical cloud model, Atmospheric Chemistry and Physics, 6, 67–80, 2006.

Twomey, S.: The influence of pollution on the shortwave albedo of clouds, Journal of the atmospheric sciences, 34, 1149–1152, 1977.

Twomey, S. and Squires, P.: The influence of cloud nucleus population on the microstructure and stability of convective clouds, Tellus, 11, 408–411, 1959.

Tzivion, S., Feingold, G., and Levin, Z.: An efficient numerical solution to the stochastic collection equation, Journal of the atmospheric sciences, 44, 3139–3149, 1987.

Tzivion, S., Reisin, T., and Levin, Z.: Numerical simulation of hygroscopic seeding in a convective cloud, Journal of applied meteorology, 33, 252–267, 1994.

van der Does, M., Knippertz, P., Zschenderlein, P., Harrison, R. G., and Stuut, J.-B. W.: The mysterious long-range transport of giant mineral dust particles, Science advances, 4, eaau2768, 2018.

Warner, C., Simpson, J., Martin, D., Suchman, D., Mosher, F., and Reinking, R.: Shallow convection on day 261 of GATE/mesoscale arcs, Monthly Weather Review, 107, 1617–1635, 1979.

Warner, J.: A reduction in rainfall associated with smoke from sugar-cane fires–An inadvertent weather modification?, Journal of Applied Meteorology, 7, 247–251, 1968.

Xue, H., Feingold, G., and Stevens, B.: Aerosol effects on clouds, precipitation, and the organization of shallow cumulus convection, Journal of the Atmospheric Sciences, 65, 392–406, 2008.

Yin, Y., Levin, Z., Reisin, T., and Tzivion, S.: Seeding convective clouds with hygroscopic flares: Numerical simulations using a cloud model with detailed microphysics, Journal of Applied Meteorology, 39, 1460–1472, 2000a.

Yin, Y., Levin, Z., Reisin, T. G., and Tzivion, S.: The effects of giant cloud condensation nuclei on the development of precipitation in convective clouds – A numerical study, Atmospheric research, 53, 91–116, 2000b.

Yuan, T.: Cloud macroscopic organization: order emerging from randomness, Atmospheric Chemistry and Physics, 11, 7483–7490, 2011.

Zhang, L., Michelangeli, D. V., and Taylor, P. A.: Influence of aerosol concentration on precipitation formation in low-level, warm stratiform clouds, Journal of aerosol science, 37, 203–217, 2006.

Zuidema, P., Li, Z., Hill, R. J., Bariteau, L., Rilling, B., Fairall, C., Brewer, W. A., Albrecht, B., and Hare, J.: On trade wind cumulus cold pools, Journal of the Atmospheric Sciences, 69, 258–280, 2012.

# Additional Supporting Information for "Sensitivity of warm clouds to large particles in measured marine aerosol size distributions – a theoretical study"

Tom Dror[1,*], J. Michel Flores[1,*], Orit Altaratz[1], Guy Dagan[2], Zev Levin[3], Assaf Vardi[4], and Ilan Koren[1]

[1]Department of Earth and Planetary Sciences, Weizmann Institute of Science, Rehovot, Israel.

[2]Atmospheric, Oceanic and Planetary Physics, Department of Physics, University of Oxford, Oxford, UK.

[3]School of Earth Sciences, Department of Geophysics, Tel Aviv University, Ramat Aviv, Israel.

[4]Department of Plant and Environmental Sciences, Weizmann Institute of Science, Rehovot, Israel.

[*]Contributed equally to this work.

**Correspondence:** Ilan Koren (ilan.koren@weizmann.ac.il)

**Contents of this file**

1. Text S1 to S8

2. Figures S1 to S8

**Introduction**

Here we show all of the marine aerosol size distributions (MSDs) that were used as inputs to the model (Text S1; Fig. S1), and the outputs of the model (i.e., rain yield and cloud's maximum mass) for the two shallower profiles used (Text S2; Fig. S2). In addition, to gain a better understanding of the non-monotonic behavior of the surface rain yield and cloud's maximum mass as a function of aerosol concentration ($N_{tot}$), we examined the time evolution of condensation–evaporation, collision–coalescence, and surface rain for the *Pacific–6* MSD (which does not contain giant or ultragiant particles; Text S3, Fig. S3). We also show, that the *Atlantic–1* MSD has no optimal aerosol concentration ($N_{op}$) by running the model with $N_{tot}$ of up to $10^6\,cm^{-3}$ (Text S4; Fig. S4). We examine the time evolution of the total droplet surface area for all MSDs at four different $N_{tot}$ (Text S5; Fig. S5), and we investigate the droplet size distributions below cloud base for all MSDs for $N_{tot} = 2629\,cm^{-3}$ (Text S6; Fig. S6). Finally, we examine the time-height evolution of the horizontal mean profiles of key parameter of the clouds (Text S7–S8; Figs. S7–S8).

**Text S1. Normalized MSDs.** Six measured MSDs that represent a variety of different marine environments were normalized to the other five MSD concentrations (total of 36 MSDs). This allowed for a careful examination of the effect of both $N_{tot}$ and the MSD's shape. Figure S1 shows all MSDs. The *Atlantic–1* and the *Atlantic–2* are the only MSDs that contained GCCN, and the *Atlantic–1* is the only MSD that contained UGCCN. Note that even though the *Atlantic—2* contained some GCCN, they were present at low concentrations ($1.6 \times 10^{-6} - 7.5 \times 10^{-5}\, cm^{-3}$, for the lowest and highest $N_{tot}$, respectively). These concentrations of GCCN are low in comparison to e.g., the GCCN concentration of the *Atlantic–1* MSD ($1.9 \times 10^{-5} - 5.7 \times 10^{-4}\, cm^{-3}$), and are not sufficient to cause any effect on the *Atlantic–2* rain formation and growth.

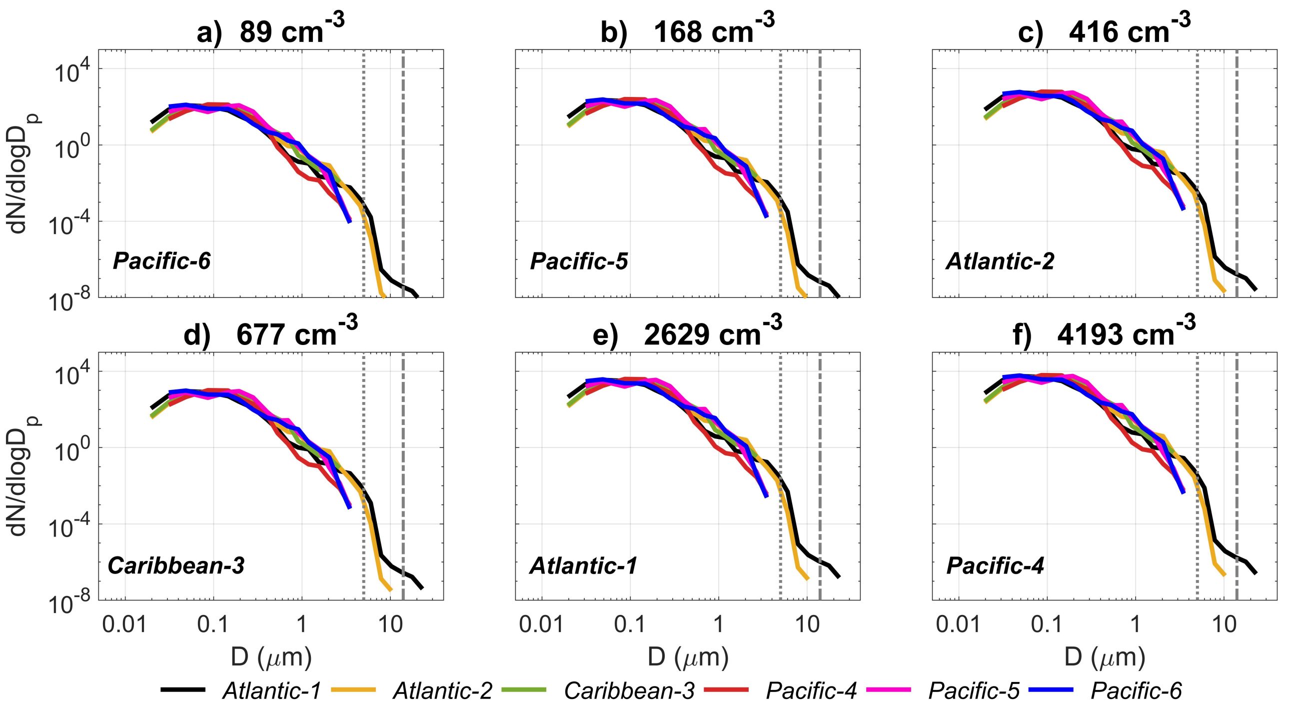


**Figure S1.** All of the MSDs used in the model. Each panel shows the MSDs normalized to the specific total aerosol concentration of the MSD noted in the lower left corner. The panels are organized from clean (a) to polluted (f) conditions. Dotted and dash-dotted verticals line indicate the threshold for GCCN ($D_p = 5\, \mu m$) and UGCCN ($D_p = 14\, \mu m$), respectively.

**Text S2. Additional Atmospheric Profiles.** To examine the effect of the different MSDs on cloud properties over a range of atmospheric conditions, we ran the model with three different sets of initial thermodynamic conditions. The initial conditions were based on idealized atmospheric profiles describing a tropical moist environment (Garstang and Betts, 1974; Dagan et al., 2015). The three profiles are presented in Figure 1 of Dagan et al. (2015) and include: a well mixed sub-cloud layer between 0 and $\sim 1000\, m$ and a conditionally unstable cloudy layer between 1000 and $4000\, m$ (deep), $3000\, m$ (intermediate), and $2000\, m$ (shallow). The profiles were bounded by an overlying inversion layer with a temperature gradient of $2^o$C over $50\, m$. Three different dewpoint temperatures were assigned to the profiles such that the relative humidity ($RH$) in the cloudy layer was

95%, 90%, and 80%, respectively. We examined the surface rain yield and the cloud's maximum mass as a function of $N_{tot}$. The results of the deepest cloud profile are shown in the main text (Fig. 2a–b), and the the other two profiles are shown in Fig. S2. The trends of the *Atlantic—1* surface rain yield and cloud's maximum mass curves for the intermediate profile are similar to the ones of the deeper profile. The only difference is that the rain yield values of the *Atlantic—1* are higher than the ones produced by the other MSDs for $N_{tot} > 677\,cm^{-3}$. All the curves show a lower $N_{op}$ compared to the deepest profile curves. Under the shallow thermodynamic profile, the *Atlantic—1* rain yield curve shows a similar trend to all other MSD cases, while producing the highest rain values. As for the trend in cloud mass, the *Atlantic—1* shows a monotonic increase (similar to the deep and intermediate profiles). The behavior of surface rain yield and the cloud's maximum mass as a function of $N_{tot}$ strongly depends on the environmental conditions, i.e., the more unstable the profile (e.g., higher inversion height and $RH$ in the cloudy layer), the more salient the revealed effect of the MSD. In all cases, the *Atlantic–1* clouds have a distinctively different behavior compared to the rest of the MSDs.

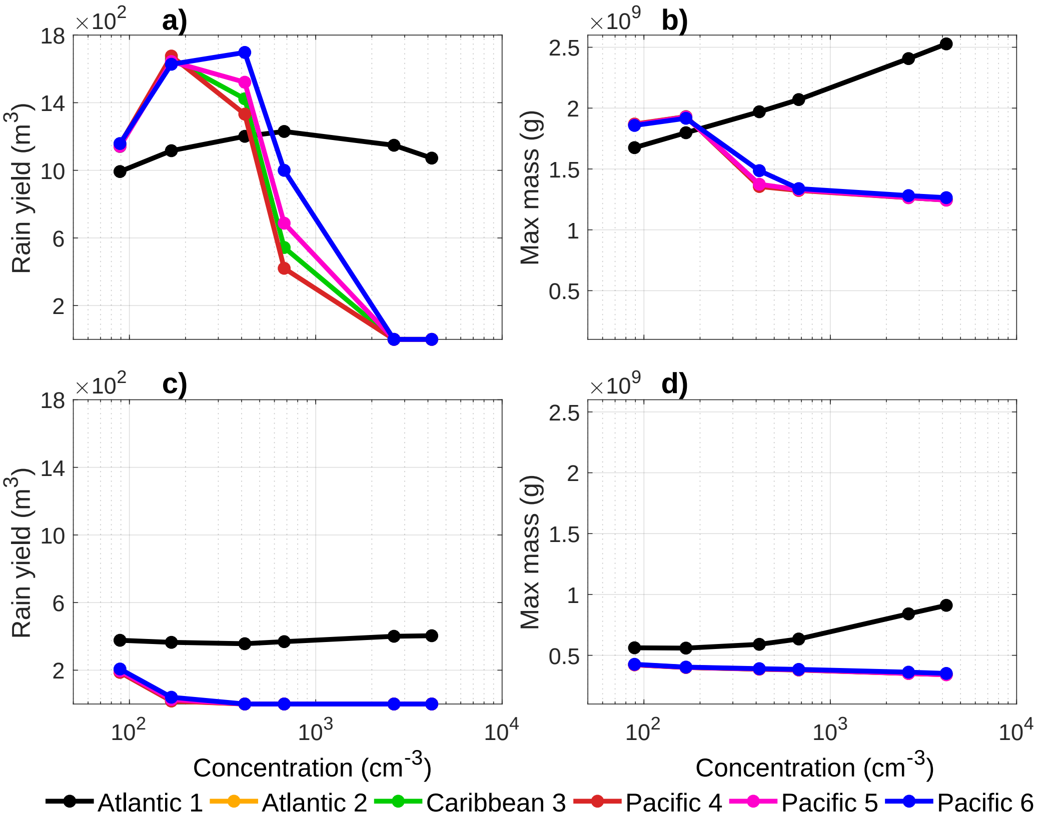


**Figure S2.** Surface rain yield (a and c) and cloud's maximum mass (b and d) as a function of $N_{tot}$ for the intermediate and shallow profiles. The top panels refer to an inversion height of $3000\,m$ and a $RH$ of 90% in the cloudy layer. The lower panels refer to an inversion height of 2000 m with 80% $RH$ in the cloudy layer. Each curve represents six simulations with a specific shape of the MSD normalized to a different $N_{tot}$.

**Text S3. Cloud's Microphysical Processes.** To understand the non-monotonic behavior of the surface rain yield and cloud's maximum mass as a function of $N_{tot}$, we examined the time evolution of condensation–evaporation, collision-coalescence, and surface rain as the three major cloud processes. Figure S3 shows these processes for three different $N_{tot}$ (clean, optimum and polluted conditions) using the *Pacific–6* MSD. The timing and the interaction between the processes are evident between the different clouds shown in Fig. SS3. As $N_{tot}$ increases (and the total droplet surface area becomes larger), so does the condensation efficiency (Pinsky et al., 2013; Seiki and Nakajima, 2014), and the collision–coalescence process is delayed. For the clean cloud, the early onset of collision–coalescence acts to further reduce the droplets' surface area, and triggers the early formation of rain. The more polluted the cloud is, the longer the time it has to grow by condensation (i.e., the peak in collision-coalescence drifts further away from the peak of condensation–evaporation). On the other hand, the delay in collision–coalescence allows entrainment processes to act for a longer time, resulting in enhanced evaporation. The cloud presented in Fig. S3b shows the evolution and interaction of these processes under an optimal $N_{tot}$ ($N_{op}$), for which the cloud mass (not shown) and surface rain yield are maximal. For the $N_{op}$ scenario, the timing of the different cloud processes is ideal for cloud growth and rain-out (Dagan et al., 2015).

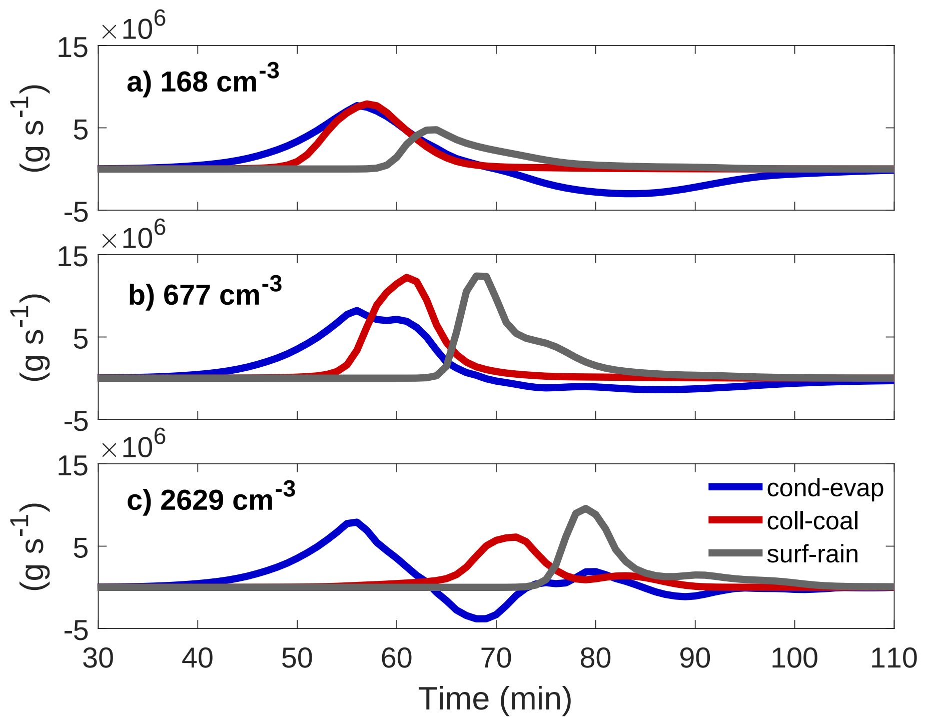


**Figure S3.** Total condensed–evaporated mass (blue), collected mass (red), and surface rain mass (gray) per unit time, as a function of time for the *Pacific–6* MSD for three different aerosol concentrations: clean (a), optimal (b), and polluted (c) for the deepest profile. The specific concentrations are noted on the upper left corner of each panel.

**Text S4. The *Atlantic–1* MSD has no $N_{op}$.** Additional sensitivity simulations were performed to examine the *Atlantic–1*'s MSD behavior under extremely polluted conditions. Figure S4 shows the same as Fig. 2a–b in the main text, but includes four additional simulations for the *Atlantic–1* MSD under $N_{tot}$ of $10^4$, $4 \times 10^4$, $10^5$, and $10^6\,cm^{-3}$. From the Figure, it is clear that a $N_{op}$ does not exist for the *Atlantic–1* MSD.

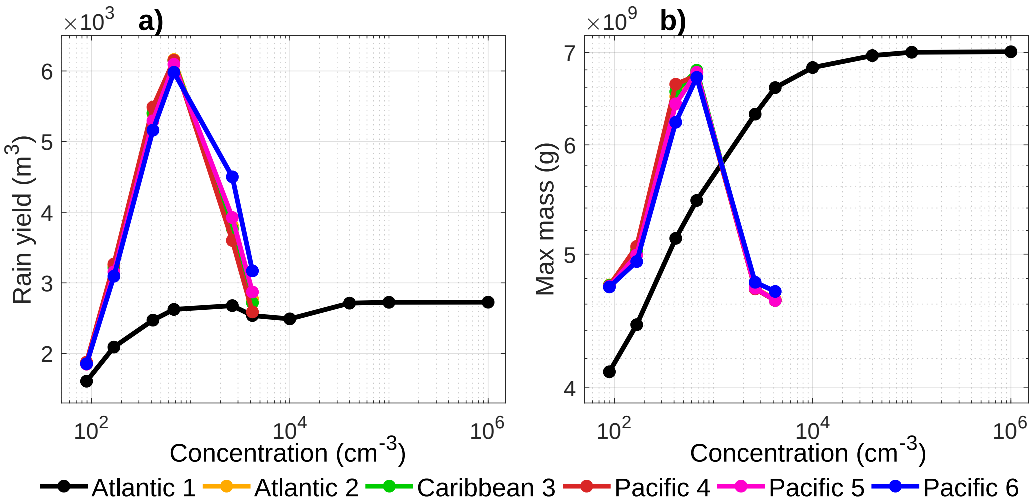


**Figure S4.** (a) Surface rain yield and (b) cloud's maximum mass as a function of $N_{tot}$ used in the simulation. Each curve represents six simulations, performed with a specific shape of the MSD normalized to a different $N_{tot}$, except for the *Atlantic–1* MSD that is comprised of 10 simulations up to an aerosol concentration of $10^6\,cm^{-3}$.

**Text S5. Total Droplet Surface Area Evolution.** The temporal evolution of the total droplet surface area (summed over all cloudy pixels) was investigated for all MSDs, for four different $N_{tot}$ (Fig. S5). The more polluted the clouds were (going from **a** to **d** in Fig. S5), the greater the difference in total droplet surface area between the *Atlantic–1* MSD and the rest of the MSDs. This is explained by the fact that the *Atlantic–1* MSD contained an UGCCN mode, and as $N_{tot}$ increased, the amount of UGCCN also increased (see Fig. S1), reducing the total droplet surface area.

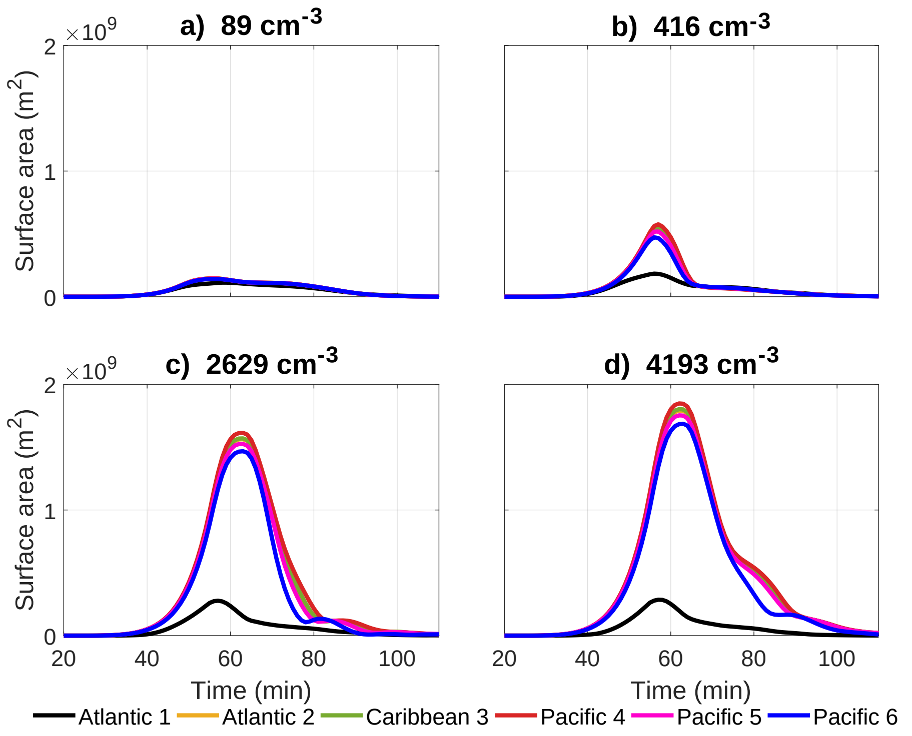


**Figure S5.** Total droplet surface area for $N_{tot}$ of (a) $89\,cm^{-3}$, (b) $416\,cm^{-3}$, (c) $2629\,cm^{-3}$ and (d) $4193\,cm^{-3}$.

**Text S6. Droplet Size Distribution Below the Cloud Base.** To understand the reduced surface rain caused by the enhanced evaporation below the cloud base of the *Atlantic–1* MSD shown in Fig. 3 of the main text, we calculated the mean droplet size distribution for the time of maximum rain for an area just below cloud base. Figure S6 shows the droplet size distribution for all of the MSDs for $N_{tot} = 2629\,cm^{-3}$. The biggest droplets in the *Atlantic–1* MSD case are about six orders of magnitude less in concentration compared to the other five MSDs, explaining the more efficient evaporation below cloud base.

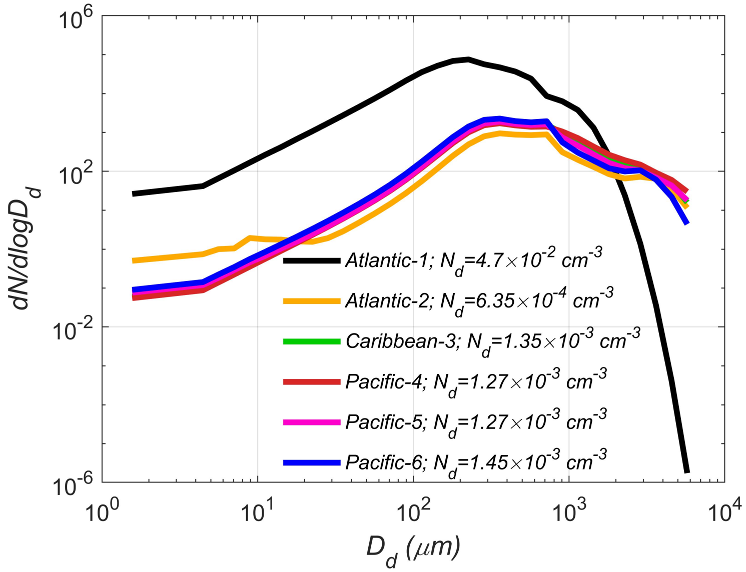


**Figure S6.** Droplet size distribution below the cloud base at the time of maximum surface rain rate for the six different MSDs normalized to $N_{tot} = 2629\,cm^{-3}$. The total droplet number concentration ($N_d$, $cm^{-3}$) is noted in the legend for each MSD.

**Text S7. Time–height Diagrams of Cloud Mean properties.** To understand the vertical distribution of some of the cloud's key properties, we show the time evolution of the cloud mass mixing ratio, droplet number concentration ($N_d$), vertical velocity ($w$), and relative humidity ($RH$) below the cloud mass of the *Atlantic–1* and the *Pacific–6* MSDs normalized to $N_{tot} = 2629\,cm^{-3}$. We show the *Pacific–6* MSD case as a representative example to the other four MSD cases, since their results are very similar. It is clear that while the *Atlantic—1*'s mass is the same order of magnitude as the one of the *Pacific–6*, the total $N_d$ is considerably smaller for the *Atlantic–1* cloud, and that the droplets are confined to the lower part of the cloud. These are big droplets that nucleated on the GCCN and the UGCCN in the *Atlantic–1* MSD. These droplets sediment out almost immediately after their formation, thus are not carried to higher levels in the cloud. The *Atlantic–1* starts to precipitate earlier than the other clouds (as discussed in the main text), while the cloud is still in its developing stage, updrafts prevail and the sub—cloud layer features low $RH$ values.

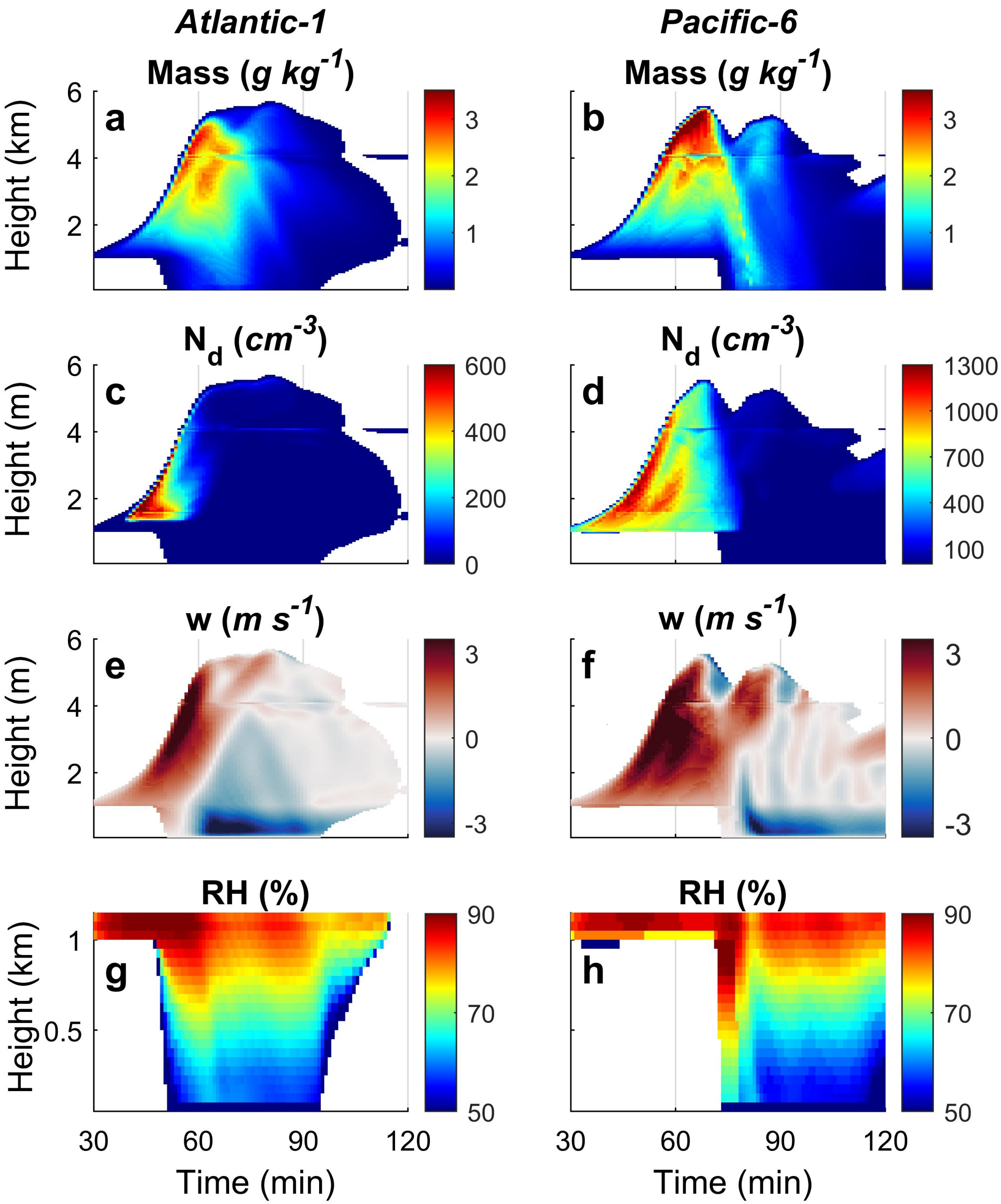


**Figure S7.** Time-height diagram of the horizontal mean of (a,b) cloud mass mixing ratio ($g\,kg^{-1}$), (c, d) droplet number concentration ($N_d$, $cm^{-3}$), (e, f) vertical velocity ($w$, $m\,s^{-1}$), and (g, h) relative humidity ($RH$, %) below the cloud base, for the *Atlantic–1* (left column) and *Pacific–6* (right column) MSDs normalized to $N_{tot} = 2629\,cm^{-3}$. Values are shown only for the cloudy (and rainy) pixels (mixing ratio $> 10^{-3}\,g\,kg^{-1}$). Note the different scales for the color bars in panels (c) and (d).

**Text S8. Time–height Diagrams of Precipitating Particle's Growth.** For clarifying the reasons behind the reduced surface rain amounts that are observed in the *Atlantic—1* MSD case, Fig. S8 shows the time-height evolution of the horizontal mean profiles of raindrops number concentration $N_r(D_p > 80\,\mu m)$, and mass mixing ratio $M_r(D_p > 80\,\mu m)$, for the *Atlantic–1* and the *Pacific–6* MSDs normalized to $N_{tot} = 2629\,cm^{-3}$. The formation of raindrops is observed at a very early stage of the *Atlantic–1* cloud lifetime, compared to the timing of the rain formation in the *Pacific–6* case. In addition, it is clear that the high $N_r$ around the *Atlantic—1*'s cloud base contains very little mass, but the drops are big enough to fall out. However, since the drops are small, and the sub—cloud layer is still dominated by updrafts (Fig. S7e–f) the majority of them evaporate before reaching the surface (efficient evaporation and longer fall time).

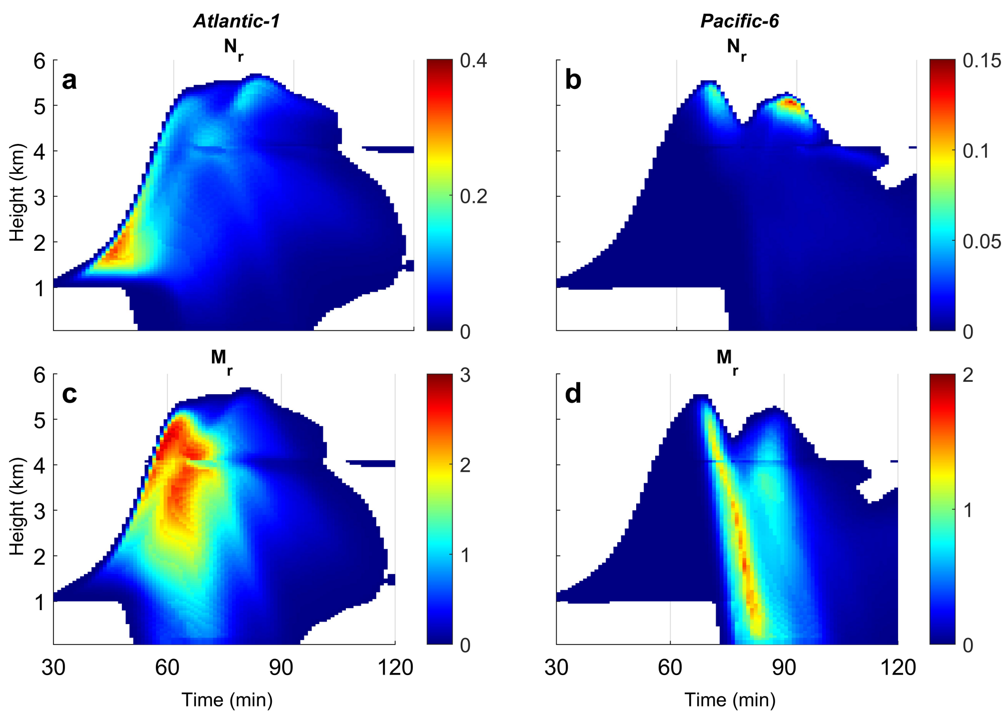


**Figure S8.** Time–height diagram of the horizontal mean of raindrops ($D_p > 80\,\mu m$) (a, b) number concentration ($N_r$, $cm^{-3}$) and (c, d) mass mixing ratio ($M_r$, $g\,kg^{-1}$), for the *Atlantic–1* (left column) and *Pacific–6* (right column) MSDs normalized to $N_{tot} = 2629\,cm^{-3}$. Values are shown only for the cloudy (and rainy) pixels (mixing ratio $> 10^{-3}g\,kg^{-1}$). Note that the color bars have different limits for the *Atlantic–1* and *Pacific–6* clouds.

## References


Dagan, G., Koren, I., and Altaratz, O.: Competition between core and periphery-based processes in warm convective clouds–from invigoration to suppression, Atmospheric Chemistry and Physics, 15, 2749–2760, 2015.

Garstang, M. and Betts, A. K.: A review of the tropical boundary layer and cumulus convection: Structure, parameterization, and modeling, Bulletin of the American Meteorological Society, 55, 1195–1205, 1974.

Pinsky, M., Mazin, I., Korolev, A., and Khain, A.: Supersaturation and diffusional droplet growth in liquid clouds, Journal of the Atmospheric Sciences, 70, 2778–2793, 2013.

Seiki, T. and Nakajima, T.: Aerosol effects of the condensation process on a convective cloud simulation, Journal of the Atmospheric Sciences, 71, 833–853, 2014.